Swiss J Geosci (2012) 105:263–282
DOI 10.1007/s00015-012-0097-1

Retrograde alterations of phyllosilicates in low-grade metapelite: a case study from the Szendrő Paleozoic, NE-Hungary

Péter Árkai · Isabel Abad · Fernando Nieto · Tibor Németh · Péter Horváth · Viktória K. Kis · Katalin Judik · Juan Jiménez-Millán

Received: 18 October 2011 / Accepted: 14 May 2012 / Published online: 2 August 2012

Abstract Frequently, at temperatures lower than the metamorphic peak conditions, slates undergo mineral transformations, usually mediated by fluids. We have studied core material of an epizonal slate series (Szendrő Mountains, NE-Hungary) to reconstruct the post-metamorphic lower-T hydrothermal alterations using petrographic, X-ray diffraction, electron microprobe methods, and transmission electron microscopy. The borehole crosscuts an upper part of the ca. 600–800 m Lower-Carboniferous flysch-like Szendrő Phyllite Formation. The samples were metamorphosed reaching epizonal conditions with a mineral assemblage characterized by quartz, muscovite, chlorite and albite. Even in the freshest samples, break-up and loosening of the regional metamorphic structure was observed, with cracks parallel to or crossing the cleavage. In the upper part, chlorite and albite are almost absent, while the presence of paragonite, mixed Na–K mica, and mixed-layered minerals with smectitic component are characteristic. Goethite, halloysite, and subordinate kaolinite are present in the most altered sample (13.0 m in the profile) which may indicate the position of the fissures in which the circulation of the post-metamorphic fluids was the most intense. Muscovite is the only mica from the lower part of the profile and chlorite becomes a significant constituent, whereas paragonite, halloysite, and kaolinite are missing. Discrete smectite is present in all the samples in spite of being incompatible with the prograde evolution of the sequence. The interleaved smectite layers in chlorite and muscovite/chlorite mixed-layers show at the lattice level textural characteristics indicative of a later alteration process. After the metamorphic peak at epizonal conditions, the introduction of hot fluids through the fractures gave rise to the crystallization of Na–K white micas and muscovite/chlorite under anchizonal conditions. In a final stage of the hydrothermal process, the cooling of the circulating fluids favored the formation of halloysite and kaolinite in the areas near to the fissures, smectites in the samples far away from the fractures, and locally, goethite. The Fe_2O_3 content increasing upwards indicates oxidizing conditions in the late stage of hydrothermal activity and/or eventually, an influence of a younger near-surface weathering.

Keywords Retrograde hydrothermal reactions · Mixed Na–K white mica · Muscovite/chlorite mixed-layers · Halloysite · XRPD · EPMA · HRTEM

Editorial handling: Sébastian Potel and Edwin Gnos.

P. Árkai (✉) · T. Németh · P. Horváth · K. Judik
Research Centre for Astronomy and Earth Sciences, Institute for Geological and Geochemical Research, Hungarian Academy of Sciences, 45 Budaörsi út, Budapest 1112, Hungary
e-mail: arkai.paksy@t-online.hu

I. Abad · J. Jiménez-Millán
Departamento de Geología, Universidad de Jaén, Unidad asociada Grupo de Geología UJA-CSIC (IACT), 23009 Jaén, Spain

F. Nieto
Departamento de Mineralogía y Petrología e IACT, Universidad de Granada, CSIC, 18002 Granada, Spain

V. K. Kis
Institute for Technical Physics and Materials Science, Hungarian Academy of Sciences, P.O.B. 49, Budapest 1525, Hungary

1 Introduction

The prograde transformations of phyllosilicates in diagenetic and low-temperature metamorphic conditions produce mostly metastable non-equilibrium assemblages.

These transformations, called reaction progress, have been intensively studied in the last 50 years (for recent comprehensive reviews see Merriman and Peacor 1999; Merriman and Frey 1999; Árkai 2002; Menuier and Velde 2004; Merriman 2005). By contrast, considerably less attention has been paid to those phyllosilicate transformations, which proceed at lower temperatures after the metamorphic peak, usually mediated by low-T hydrous fluids. The processes that proceed under diagenetic conditions were named "retrograde diagenesis" by Nieto and Peacor (1993). Nieto et al. (2005) systematically reviewed the known examples of retrograde diagenesis. These authors concluded that retrograde reactions affecting low-T metamorphic phyllosilicates are more common than generally assumed. For recognizing such reactions and their mineral products, application of X-ray powder diffractometric (XRPD), electron probe microanalysis (EPMA) and conventional petrographic microscopic methods is required together with high-resolution transmission electron microscopy (HRTEM) and energy dispersive spectrometer (EDS) assisted transmission electron microscopy (STEM). In addition to retrograde diagenesis, phyllosilicate retrogression may occur also in lower-T regional metamorphic, hydrothermal, metasomatic or local tectonic (cataclastic) regimes (Abad et al. 2003; Jiménez-Millán et al. 2007).

The present paper describes and evaluates a rather specific example of an epizonal slate series that underwent post-metamorphic lower-T hydrothermal alterations. The main aim is to reconstruct these processes and to characterize the mineral products. Special attention is paid to the characterization of the regional metamorphic assemblage, to the changes in structural and chemical features of phyllosilicates, and to the bulk rock major element chemistry. The changes in metamorphic zone indicated by the characteristics of K-white mica and chlorite and the formation of paragonite, hydrous Al-silicates (halloysite and kaolinite), and a peculiar mixed-layer phyllosilicate at the expense of regional metamorphic minerals will be discussed in detail.

2 Geological setting and materials

The Szendrő Mountains are located within the Alpine–Carpathian–Pannonian–Dinaridic mountain chain (Fig. 1a). The Paleozoic formations of the Szendrő Mountains form part of the Bükk Unit within the Pelso Unit. The Bükk Unit shows clear lithological, biostratigraphic, and paleogeographical affinities to the Inner Dinarides, although considering its present tectonic position it forms the innermost unit of the Western Carpathians (for details see Kovács et al. 2000).

The rock samples presented in this paper derive from a ca. 90 m deep borehole Gn-1 near the village Gadna in the southeastern part of the Szendrő Mountains, northeastern Hungary (Fig. 1b). According to Fülöp (1994), the borehole crosscuts an upper part of the ca. 600–800 m thick Szendrő Phyllite Formation that represents a flysch-like sedimentation of Lower Carboniferous age (Fig. 2). Phyllites and slates of this formation are built up mainly by pelitic-silty metasedimentary rocks. They originated from chemically only weakly weathered (immature: originally rich in feldspars and biotite) detritus that deposited in a mobile basin, in the foreland of the European Variscan orogenic belt (Árkai 1977a, b, 1982).

The Paleozoic and Mesozoic formations of the Bükk Unit suffered very low- to low-grade (anchi-, epizonal) regional (orogenic) metamorphism (Árkai 1977b, 1983). Comparing the metamorphic zone- (temperature-) and pressure-indicating parameters in the whole Bükk Unit (Bükk, Uppony, and Szendrő Mountains) in a profile ranging from Silurian up to the Jurassic, Árkai (1983) proved the existence of only one (Alpine, Cretaceous, pre-Senonian) dynamothermal regional metamorphic event. Variscan event could not be evidenced; in the case of existence, it would have been obliterated by the Alpine event, which culminated between the eo-Hellenic phase (ca. 160–120 Ma) and the Austrian phase (ca. 100–95 Ma) (Árkai et al. 1995a). Therefore, the metamorphic grade of an eventual Variscan event would have been lower than that of the Alpine metamorphism.

In this paper, 11 rock samples were selected from the borehole based on previous mesoscopic, petrographic microscopic and XRPD investigations (Árkai 1977a), which allowed a first vertical subdivision of this sequence using the signs of post-metamorphic low-T alteration processes. Out of these, four samples were selected and studied by EPMA and HRTEM. They represent the quasi unaltered regional metamorphic slate, the moderately or strongly altered (hydrothermally destructed) slate, and that in which the hydrothermal alteration was the strongest.

3 Methods

Conventional petrographic meso- and microscopic observations were aimed at the determination of rock types, with special reference to the discrimination of detrital (inherited), metamorphic, and post-metamorphic minerals and syn- and post-metamorphic microstructural features.

The XRPD, EPM and bulk rock chemical analyses were carried out in the Institute for Geological and Geochemical Research, Hungarian Academy of Sciences, Budapest. XRPD patterns were obtained from both non-oriented and highly-oriented powder mounts of whole-rock samples and their <2 μm spherical equivalent diameter (SED) size fractions, using a Philips PW-1730 diffractometer with computerized APD system. Air-dried (AD), glycolated

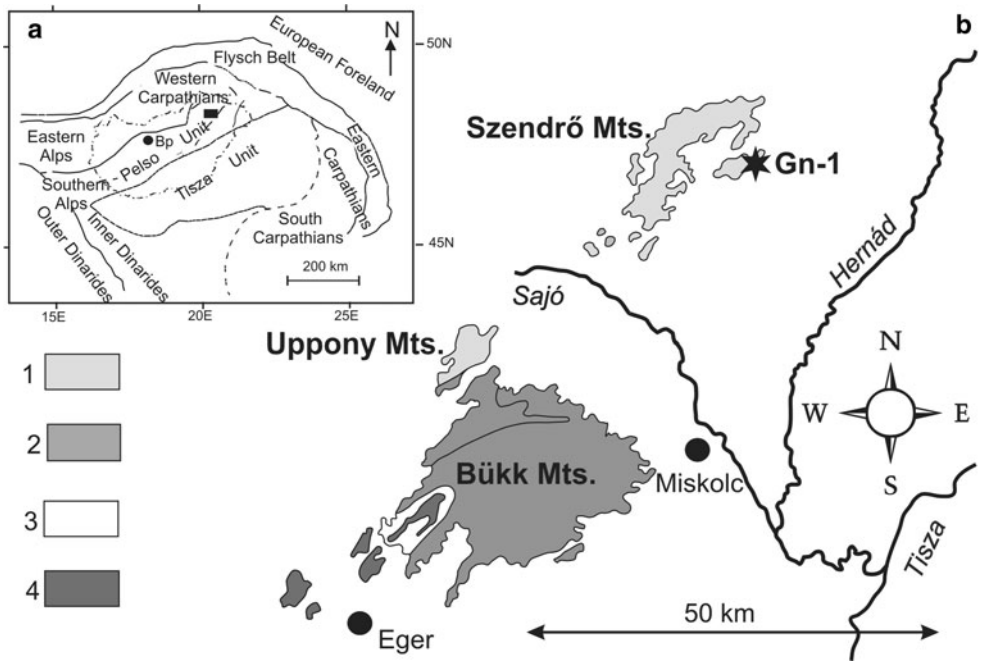

Fig. 1 **a** Tectonic frame of the Alpine–Carpathian–Pannonian–Dinaridic realm. For rough orientation the state boundary of Hungary is indicated by *dash-dot line*. *Bp* Budapest; **b** Geological sketch map of the Szendrő Mountains with the location of the borehole Gadna Gn-1. *1* Paleozoic (Ordovician to Lower Carboniferous) mostly metasedimentary formations of the Szendrő and Uppony Mountains; *2* Parautochthonous unit of the Bükk Mountains (Middle Carboniferous to Jurassic); *3* Jurassic sedimentary formations of the Szarvaskő–Mónosbél Nappe of the Bükk Mountains; *4* Ophiolitic sequences of the Szarvaskő–Mónosbél Nappe

(EG), glycerol-solvated, Mg-, K- and Li-saturated (with 0.5 and 1 N chloride solutions) and heated (up to 250, 350 and 550 °C) mounts were obtained and studied, and the Green-Kelly test (Green-Kelly 1953) for the possible most precise determination of the swelling components in the mixed-layered phases was carried out. The procedures of sample preparation and treatments, as well as the XRPD instrumental and measuring conditions and their errors, were described in detail by Árkai et al. (2002) and Németh et al. (1999). XRPD data were used for the determination of mineral phases, modal compositions of rocks, and values of illite-muscovite Kübler index and chlorite "crystallinity" indices (KI and ChC, respectively). The calibration of KI and ChC values to Kübler's KI scale was made using standard rock slab series provided by B. Kübler, and the least-squares method was used so that the KI boundaries of the anchizone corresponded exactly to 0.25 and 0.42°Δ2Θ. Consequently, the anchizone boundaries of ChC(001) and ChC(002) in the present paper are 0.26–0.38 and 0.24–0.30°Δ2Θ for fine-clastic metasedimentary rocks (Árkai et al. 1995b). For further details of the calibration see Kisch et al. (2004).

Major element compositions of bulk rock samples were determined using Perkin Elmer 5000 and Perkin Elmer Analyst 300 atomic absorption spectrophotometers (AAS), after digestion with lithium metaborate. In addition to AAS, spectrophotometric, permanganometric (FeO), gravimetric (SiO_2, TiO_2, H_2O, and P_2O_5) and volumetric (CO_2) methods were applied.

Electron probe microanalyses (EPMA) of phyllosilicates and other rock-forming minerals were performed on selected rock samples using a Jeol JCXA-733 electron microprobe equipped with an Oxford INCA 200 EDS. Operating conditions were 20 keV accelerating voltage, 4 nA sample current, 100 s counting time and 5 μm beam diameter. The following standards were used: albite (Na), quartz (Si), corundum (Al), periclase (Mg), orthoclase (K), apatite (Ca), hematite (Fe), spessartine (Mn) and rutile (Ti).

The HRTEM studies were carried out with a Philips CM20 (STEM) operating at 200 kV (Centro de Instrumentación Científica, C.I.C., Universidad de Granada) and a JEOL3010 TEM equipped with GIF system operating at 300 kV (Institute for Technical Physics and Materials Science, Hungarian Academy of Sciences, Budapest). Cu rings were attached to representative areas of the thin sections. These areas were detached through gentle heating and further thinned with a Gatan dual ion mill. Analytical electron microscopy (AEM) was applied to obtain quantitative chemical analyses of particles' thin edges in the STEM mode with an EDAX microanalysis system. Moreover, powders of the selected samples were dispersed in ethanol and the resulting suspension was dropped onto lacey prepared using holey C-coated Cu grids and subsequently analysed also with a Philips CM20 TEM equipped with a Noran EDS. The analyses performed on individual particles allow a larger area to be used and provides better reproducibility of data due to the decrease in alkali loss. Albite, olivine, biotite, spessartine, muscovite, chlorite, and titanite were used to obtain k-factors for transformation of intensity ratios to concentration ratios according to the Cliff and Lorimer (1975) approximation.

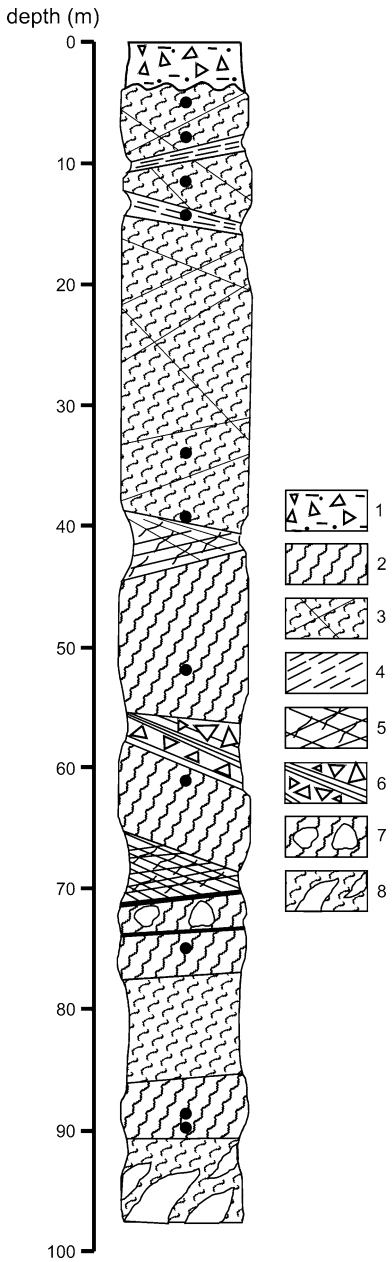

Fig. 2 Geologic and petrographical profile of the borehole Gn-1 with the samples investigated. *1* Soil with weathered detritus of the bedrock; *2* dark-grey, blackish-grey fresh slate; *3* grey, brownish-grey altered and fractured slate; *4* yellowish-grey, light-grey, strongly altered slate; *5* very strongly altered and fractured slate; *6* very strongly altered and fractured slate with blocks of relatively fresh slate; *7* dark-grey, silicified slate with several cm large white quartzite lenses, the latter showing evidence of corrosion; *8* whitish-grey, white smectitic clay (alteration product of slate) with quartzitic lenses that contain sulfide minerals (mainly, pyrite)

4 Results

4.1 Petrography

The fresh phyllites and slates of the Lower Carboniferous Szendrő Phyllite Formation are dark-grey, fine- to very fine-grained, and generally display two cleavage plane sets. The first foliation is usually parallel with the sedimentary bedding. This foliation is micro-folded (crenulated). The sizes of microfolds are in 0.1–1 mm orders of magnitude. Intense shear that acted in the limbs of asymmetric microfolds developed crenulation cleavage that was accompanied by re-arrangement of minerals recrystallized or newly formed. A characteristic example of silty-pelitic phyllite from the *locus classicus* of the formation is displayed in Fig. 3a. In the regional metamorphic phyllites and slates, phyllosilicates (exclusively K-white mica and chlorite) and opaques (pyrite, graphite-d_1, finely dispersed organic matter, rarely hematite) are accumulated in or close to the cleavage planes (p-domains), while the inter-cleavage parts (q-domains) contain recrystallized or newly formed quartz, albite, small amounts of calcite, as well as phyllosilicate platelets among them.

In the profile of the borehole Gn-1 the intervals that contain rather fresh metamorphic rocks are represented by dark-grey, black pelitic-silty, rarely pelitic-carbonatic slates with crenulation cleavage. Even in the freshest samples (see, e.g., Fig. 3b) break-up, loosening of the regional metamorphic structure, i.e., fracturing, fracture-filling and gradual disappearance of foliation can be observed. The cracks run parallel with or cross the cleavage plains and are filled with light-grey, whitish-grey material that—under the petrographic microscope—is built up by aggregates of thick-set, idioblastic white mica, and quartz grains without any preferred orientation (Fig. 3c).

Where the fracturing becomes more intense, in the white, light-grey lenses, bands or fissure fillings again the thick white mica flakes, quartz grains and other phyllosilicates prevailed (Fig. 3d). These grains are arranged randomly (Fig. 3e) that refers to crystallization in a strain-free medium or space. In the rocks with the strongest post-metamorphic alteration quartz, hydrous Al-silicates and locally, goethite are the main phases. The traces of original regional metamorphic microstructure are still visible (Fig. 3f).

4.2 XRPD data

The mineralogy of the studied samples is given in Table 1. There are systematic differences between the upper and lower parts of the borehole profile. From samples 4.1–34.0 m chlorite and albite are absent, while the presence of paragonite, halloysite (accompanied by kaolinite on the basis of TEM observations) and mixed-layered clay minerals (ML) with various amounts of swelling smectitic component or discrete smectite phase as well as goethite are characteristic. Quartz and white mica (predominantly muscovite, subordinately paragonite) are common constituents of this upper section. Sample 13.0 m shows the most intense post-metamorphic alteration, having the highest quartz content with minor amounts of halloysite and goethite

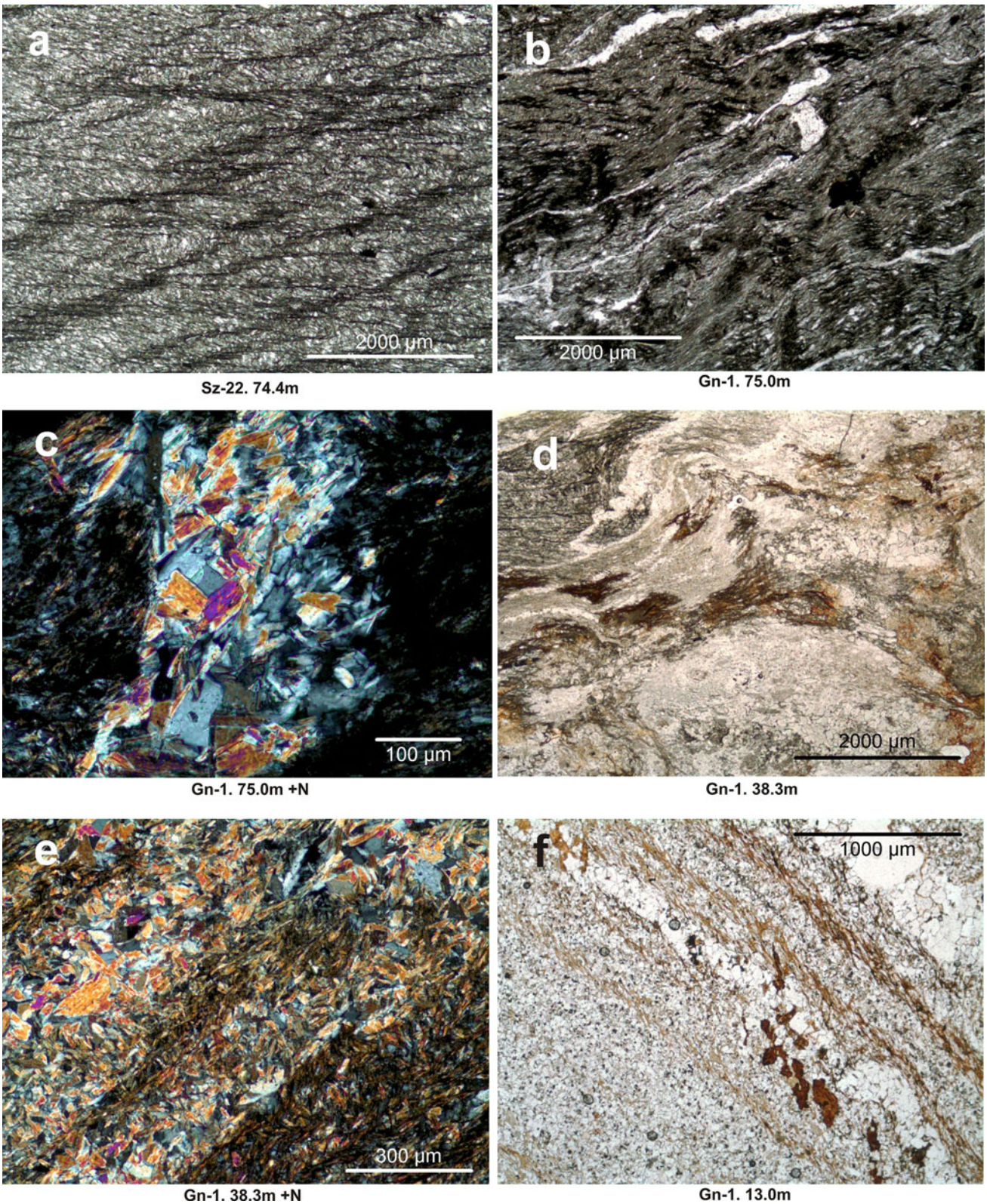

Fig. 3 Microstructural features of slate samples from borehole Gn-1, indicating the depth of each sample (photos **b–f**). For comparison a typical phyllite of pelitic-silty origin from the *locus classicus* of the Szendrő Phyllite Formation (borehole Szendrő Sz-22) is also shown (**a**). For explanation see the text. *+N* crossed polars

Table 1 Modal compositions of the metamorphosed, hydrothermally altered metapelite samples from bore Gadna Gn-1, Szendrő Paleozoic, NE-Hungary

Sample	Whole rock samples													<2 μm grain-size fraction samples												
	Qtz	Ab	Ms	Pg	MWM	Chl	Hys	Sm	ML	V	Cal	Py	Hem	Goe	Rt	Qtz	Ab	Ms	Pg	MWM	Chl	Hys	Sm	ML	V	Cal	Py	Hem	Goe	Rt
4.1 m	x		x	0	tr		x	tr	0					0	?	0		+	0	tr		x	0	x					0	?
7.6 m	x		x	0	tr		x		0					0	?	0		x	0	tr		x	tr	x					0	?
10.6 m	x		x	0	tr		x		0						?	x		+	x	tr		x	0	x					0	?
13.0 m	+	0	x	0	tr		x	0		0	tr			tr	?			x	0	tr		+	0		0				0	?
34.0 m	x	tr	x	0	tr	tr	x		0		tr		?	tr	?	x		x	x	tr	tr	x		0		0			0	?
38.3 m	x		x	0	tr	0	0	0	tr						?	0		x	0	tr	x	0	0	0		0		tr	0	?
52.0 m	x	x	x		tr	x		0	tr			tr?			tr	0	0	x		tr	x		0	0		0				0
60.0 m/b	x	0	x		tr	x					x				tr	0	0	x		tr	x		0	0		0			0	0
75.0 m	x	tr?	x		tr	x		0	tr						tr	x		+		tr	x		0	x		0				0
89.0 m/a	x	x	x		tr	x					x	tr?			tr	x	0	x		tr	+		0	0		0	0		0	0
89.0 m/b	x	x	x		tr	x		0			x				tr	0	tr?	x		tr	x		x	x					0	0

Abbreviations of mineral names after Siivola and Schmid (2007) except *Hys* halloysite, *MWM* mixed Na–K-white mica, *Sm* smectite, *ML* mixed-layered clay mineral (mostly chlorite/muscovite) and *V* vermiculite (see text)

+, dominant; x, significant; 0, subordinate; tr, traces; ?, questionable

in the bulk rock fraction. This quartz is present as secondary aggregates with relatively large grain-size. From sample 34.0 m downwards chlorite appears as traces and in subordinate quantities and becomes a significant constituent from sample 52.0 m downwards. Simultaneously, muscovite will be the only white mica in this lower part of the profile. Notwithstanding, irregularly, subordinate amounts of discrete, well swelling, tetrahedral charged (beidellitic) smectite and/or ML appear also in this lower part according to the glycerol solvation after Mg-saturation, glycolation and the results of the Green-Kelly test. As to XRPD patterns, samples 60.0, 75.0 and 89.0 m/a are the relatively freshest ones showing a rather simple and stable metamorphic phyllosilicate assemblage of muscovite + chlorite, without paragonite and kaolinite group minerals (Fig. 4a; sample 75.0 m). Some of the samples contain also minor or significant amounts of calcite.

The <2 μm fractions of the samples 4.1, 7.6, 10.6, 34.0 m, and partly that of the 38.3 m sample, representing the upper part of the profile, except sample 13.0 m, exhibit complicated XRPD patterns and are rather similar to each other. As shown in Fig. 4b (sample 4.1 m), muscovite and halloysite are the predominant phases, clarified by the intense, sharp reflection at 10 Å, and by the broad peak at 7.3 Å, respectively. Smaller amounts of paragonite are also present based on the reflection at 9.7 Å and the position of the hkl (0010) reflection. However, the 12–13 Å and corresponding near-8 Å reflections are the most characteristic features of the XRPD patterns obtained from these samples. The broad reflection around 12.6 Å (with a shoulder towards lower 2θ angles) partially shifted to 17 Å upon glycolation. Additionally, this peak shifted to 14.3 Å and increased its intensity after Mg-saturation, but did not expand after subsequent glycerol-solvation. Upon heating at 550 °C it shifted and remarkably sharpened and increased at 12 Å. The near-8 Å reflection (that provisionally may refer to the (003) reflection of a 24 Å superstructure) did not change its position, shape, and intensity upon glycolation, K-saturation, Li-saturation, the Green-Kelly test or applying heat treatments at 250 and 350 °C, but its intensity strongly decreased at 550 °C. By Mg-saturation it shifted towards the 7 Å reflection increasing the intensity of the latter one, and no changes could be observed after glycerol treatment of the Mg-saturated samples. All these features of the ca. 12.6 Å and ca. 8 Å reflections refer to interstratification of 10 Å (muscovite) and not swelling 14 Å (chlorite) layers (ML) with certain (usually subordinate) amounts of also mixed-layered swelling 14 Å (vermiculitic and/or smectitic) component and/or discrete swelling phases. In some samples the shift of low-angle shoulder of the 12.6 Å reflection to 17 Å after glycolation may refer to the presence of discrete smectite phase.

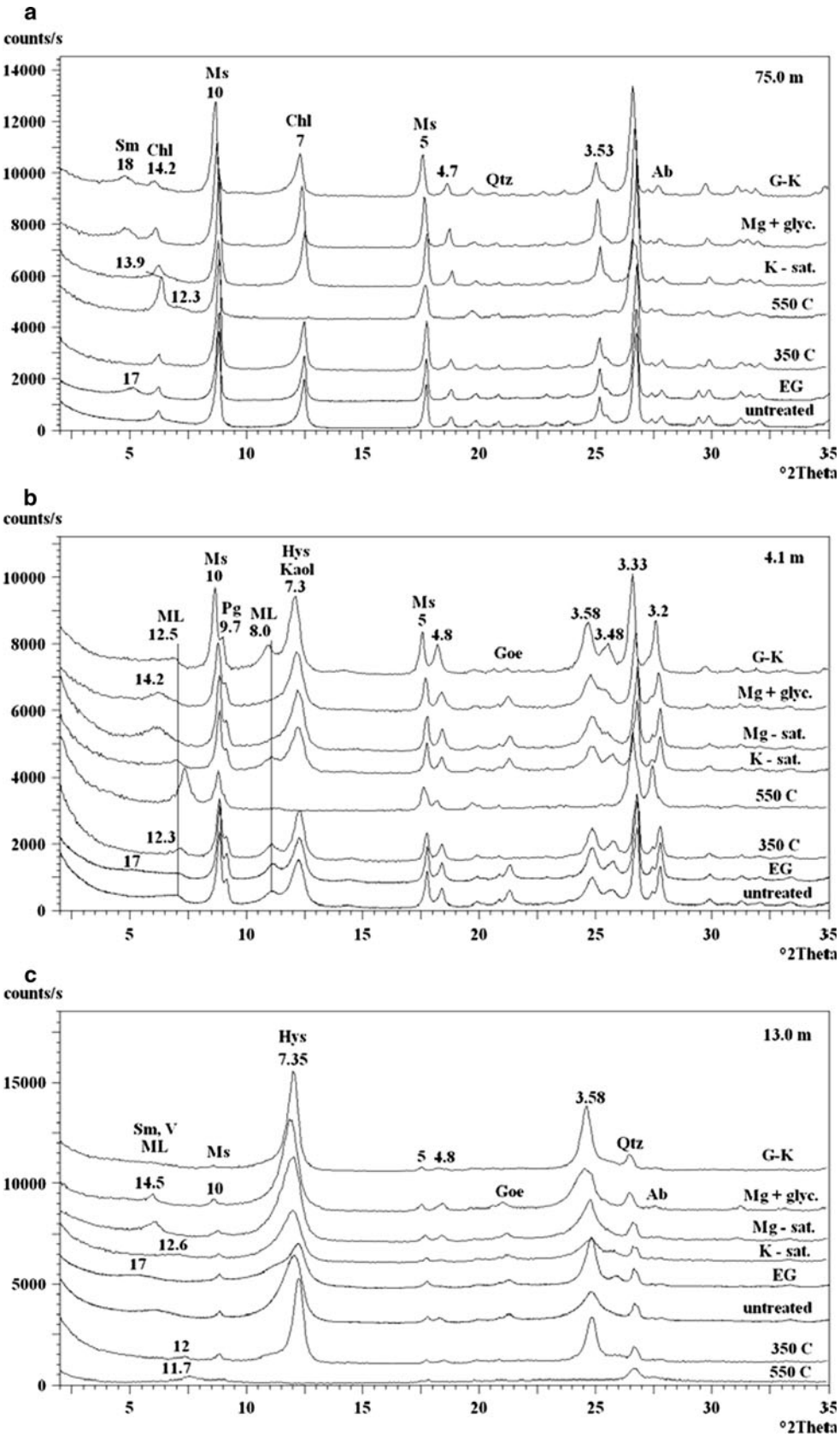

Fig. 4 XRPD patterns of the <2 μm fraction of sample 75.0 m (**a**), sample 4.1 m (**b**) and sample 13.0 m (**c**). **d** Spacings in Å are indicated. *EG* ethylene glycol solvated, *350 C and 550 C* heated to 350 and 550 °C, *K-sat.* potassium saturated, *Mg-sat.* magnesium saturated, *Mg + glyc.* Mg-saturated and glycerol solvated, *G-K* Green-Kelly test. Abbreviations of mineral names: *Sm* smectite; *V* vermiculite; *ML* mixed-layered muscovite/chlorite; *Chl* chlorite; *Kaol* kaolinite; *Hys* halloysite; *Ms* illite-muscovite; *Pg* paragonite; *Goe* goethite; *Qtz* quartz (For further explanation see the text)

Table 2 Illite Kübler index (KI) and chlorite "crystallinity" (ChC) values of the <2 μm grain-size fraction samples (data in Δ°2θ) and *b* cell dimension data of illite-muscovite (whole-rock samples)

Sample	Illite Kübler index (KI) and chlorite "crystallinity" [ChC(001) and ChC(002)] values												Ill-Ms *b* cell dimension (Å) (whole-rocks)
	Air-dried (AD)						Ethylene glycol-solvated (EG)						
	Ill-Ms 10 Å		Chl 14 Å		Chl 7 Å		Ill-Ms 10 Å		Chl 14 Å		Chl 7 Å		
	FWHM	KI	FWHM	ChC(001)	FWHM	ChC(002)	FWHM	KI	FWHM	ChC(001)	FWHM	ChC(002)	
Gn-1 4.1m	*0.23*	*0.24*	–	–	–	–	*0.21*	*0.22*	–	–	–	–	8.989
Gn-1 7.6m	*0.22*	*0.24*	–	–	–	–	*0.24*	*0.25*	–	–	–	–	8.987
Gn-1 10.6m	*0.22*	*0.23*	–	–	–	–	*0.20*	*0.22*	–	–	–	–	8.981
Gn-1 13.0m	*0.21*	*0.22*	–	–	–	–	*0.21*	*0.22*	–	–	–	–	–
Gn-1 34.0m	*0.21*	*0.23*	–	–	–	–	*0.21*	*0.22*	–	–	–	–	8.986
Gn-1 38.3m	*0.22*	*0.24*	–	–	–	–	*0.22*	*0.24*	–	–	–	–	8.987
Gn-1 52.0m	0.20	0.21	–	–	0.28	0.29	0.20	0.22	–	–	0.30	0.31	8.989
Gn-1 60.0m/b	0.19	0.20	0.19	0.21	0.19	0.21	0.19	0.21	0.20	0.21	0.18	0.19	–
Gn-1 75.0m	0.20	0.21	–	–	0.26	0.27	0.20	0.22	–	–	0.24	0.26	8.992
Gn-1 89.0m/a	0.21	0.23	0.23	0.24	0.21	0.22	0.20	0.22	0.21	0.23	0.20	0.22	–
Gn-1 89.0m/b	0.20	0.22	–	–	0.20	0.22	0.20	0.21	–	–	0.21	0.22	–

FWHM: as measured full width at half maximum height of the basal reflection; with italic: FWHM and KI values of samples that contain Pg in subordinate quantities to Ill-Ms. *Equation used for calibration:* KI or ChC = 0.9430 × FWHM + 0.0269 (r = 0.9998) for further details of the calibration see Kisch et al. (2004)

The <2 μm grain-size fraction of sample 13.0 m (i.e., the sample with the strongest post-metamorphic transformation) consists predominantly of halloysite (Fig. 4c). This phase is accompanied only by small amounts of muscovite, paragonite, smectite, vermiculite, goethite, and (in the whole-rock sample) quartz. The first basal reflection of halloysite is at 7.35 Å indicating that this phase is a dehydrated 7 Å halloysite. The (001) reflection of halloysite did not change upon cation saturation, glycerol solvation, and glycolation. In sample 13.0 m EG-solvation produced a very broad reflection at 16.5 Å and a well determinable 7.8 Å shoulder beside the 7.2 Å peak. Heating at 350 °C remarkably sharpened the first basal reflection of halloysite, and further heating to 550 °C lead to the disappearance of the 7.2 Å peak. As it was evidenced by Mg-saturation and subsequent glycerol solvation, the swelling phases are smectite and vermiculite. The shift of smectite peak to 12.6 Å after K-saturation indicates that this smectite has low layer charge. Upon heating the smectite and vermiculite in this sample are more stable than the typical smectite and vermiculite. This phenomenon refers to the presence of interstratification of (small amounts of) chloritic layers within these swelling minerals (Fig. 4c).

The metamorphic zone-indicating illite Kübler index (KI) and chlorite "crystallinity" index [ChC(001) and ChC(002)] values and their statistical parameters are given in Table 2. Glycolation has practically no effect on the KI values. The illite-muscovite (K-white mica) *b* cell dimension (=6*d(060,33 $\bar{1}$) values of rock samples the modal compositions of which are adequate for qualitative indication of pressure ranges (samples 52.0 and 75.0 m) vary between 8.989 and 8.992 Å.

4.3 Bulk-rock chemical composition

Bulk rock major element compositions are given in Table 3. Part of these data was evaluated and discussed in detail by Árkai et al. (2008), mainly in relation to the occurrence or absence of paragonite and/or mixed K–Na white mica in addition to muscovite in diagenetic to low-temperature metamorphic terranes. The data have been compared with the average of Post-Archaean Australian Shales (PAAS) (Taylor and McLennan 1985) commonly used as a reference shales. The data for samples of this study are close to them although opposite changes in SiO_2 and Al_2O_3 contents and relatively high Al_2O_3 content especially in the upper part of the sequence are observed. In addition, the loss on ignition (LOI) is large in some of the samples in which the presence of calcite (Table 1) is significant. The Fe_2O_3 content increases whereas the FeO content decreases upwards and very small-scale fluctuation in Na_2O, and by contrast large fluctuation in K_2O can be demonstrated. In spite of these differences, the analyzed samples are representative of the average pelitic rock.

Table 3 Bulk rock major element compositions (in weight-%)

Sample	SiO_2	TiO_2	Al_2O_3	Fe_2O_3	FeO	MnO	MgO	CaO	Na_2O	K_2O	H_2O^-	H_2O^+	CO_2	P_2O_5	Total	LOI
4.1 m	52.34	1.11	27.37	4.38	0.69	0.03	1.03	0.11	1.13	4.66	0.39	5.92	0.00	0.06	99.22	5.84
7.6 m	49.46	1.05	26.75	6.78	0.49	0.07	1.57	0.19	0.86	4.72	0.91	6.97	0.00	0.11	99.93	6.92
10.6 m	57.08	1.11	25.75	2.37	0.35	0.02	0.84	0.10	1.05	5.15	0.39	5.58	0.00	0.06	99.85	5.54
13.0 m	78.18	0.41	9.83	3.54	0.34	0.02	0.90	0.13	0.66	0.90	0.52	3.68	0.00	0.07	99.17	3.64
34.0 m	54.47	1.07	24.86	3.96	1.56	0.05	1.42	0.14	1.35	5.00	0.50	5.64	0.00	0.08	99.92	5.47
38.3 m	60.21	0.99	21.47	2.36	2.01	0.06	0.86	0.16	0.87	3.96	0.38	5.63	0.44	0.07	99.47	5.85
52.0 m	59.94	0.90	18.10	1.54	4.74	0.05	3.06	0.33	2.33	2.17	0.49	5.06	0.00	0.10	98.81	4.53
60.0 m/b	47.66	0.63	9.11	0.65	3.97	0.19	3.45	14.17	0.76	1.50	0.14	4.25	10.54	0.12	97.14	14.35
75.0 m	47.75	1.29	27.68	1.24	4.25	0.05	2.10	0.46	0.75	6.20	0.32	6.81	0.00	0.08	98.98	6.34
89.0 m/a	58.22	0.36	4.86	1.19	4.64	0.41	1.79	11.36	1.34	0.42	0.14	2.55	9.54	0.08	96.90	11.57
89.0 m/b	50.26	0.94	21.63	1.59	5.61	0.07	3.41	1.84	0.54	4.61	0.88	5.79	1.37	0.12	98.66	6.54

Table 4 Electron probe microanalyses of white micas (cation numbers normalized to $O_{10}(OH)_2$)

Sample	Mineral	n		Si	Al^{IV}	Al^{VI}	Ti	Fe^{2+}	Mn	Mg	Ca	K	Na	Total	$\sum$ oct.	$\sum$ inter.	t.i.c.	Al^t	#Mg
75.0 m	Ms	13	Mean	3.11	0.90	1.86	0.02	0.08	0.00	0.07	0.00	0.79	0.15	6.97	2.03	0.94	0.94	2.76	48.79
			SD	*0.04*	*0.04*	*0.03*	*0.01*	*0.04*	*0.01*	*0.03*	*0.00*	*0.05*	*0.05*	*0.04*	*0.03*	*0.06*	*0.06*	*0.07*	*13.22*
38.3 m	Ms	3	Mean	3.10	0.90	1.92	0.00	0.05	0.00	0.04	0.00	0.77	0.20	6.98	2.01	0.97	0.97	2.81	46.17
			SD	*0.00*	*0.00*	*0.02*	*0.00*	*0.01*	*0.00*	*0.01*	*0.00*	*0.02*	*0.03*	*0.03*	*0.01*	*0.04*	*0.04*	*0.02*	*11.76*
	Pg	3	Mean	2.99	1.01	2.01	0.00	0.00	0.00	0.00	0.02	0.08	0.85	6.96	2.01	0.95	0.97	3.02	–
			SD	*0.04*	*0.04*	*0.03*	*0.00*	*0.00*	*0.00*	*0.00*	*0.02*	*0.01*	*0.10*	*0.09*	*0.03*	*0.11*	*0.12*	*0.02*	–
13.0 m	Ms[b]	1	repr. anal.	3.15	0.85	2.13	0.00	0.05	0.00	0.00	0.00	0.32	0.05	6.55	2.18	0.37	0.37	2.98	0.00
7.6 m	Ms	1	repr. anal.	3.17	0.83	1.90	0.00	0.07	0.00	0.08	0.00	0.66	0.17	6.88	2.05	0.83	0.83	2.72	54.57
	Ms-Pg[a]	1	repr. anal.	3.08	0.92	1.98	0.00	0.05	0.00	0.02	0.04	0.23	0.54	6.85	2.05	0.80	0.84	2.90	24.44

n number of the measured grains, *repr. anal.* representative analysis, *SD* standard deviation (with italic), $\sum$ *oct.* sum of octahedral cations, $\sum$ *inter.* sum of the interlayer cations, *t.i.c.* total interlayer charge = 2 × Ca + K + Na, Al^t sum of Al^{IV} and Al^{VI}, *#Mg* Mg/(Mg + Fe^{2+}) × 100

[a] Finely intergrown Ms and Pg phases

[b] Strongly degraded Ms

Table 5 Electron probe microanalyses of chlorites (cation numbers normalized to $O_{10}(OH)_8$)

Sample	Mineral	n		Si	Al^{IV}	Al^{VI}	Fe^{2+}	Mn	Mg	Ca	K	Na	Total	$\sum$ oct.	$\sum$ inter.	t.i.c.	Al^t	#Mg
75.0 m	Chl	5	Mean	2.63	1.37	1.56	2.51	0.01	1.83	0.00	0.00	0.00	9.90	5.90	0.00	0.00	2.93	42.13
			SD	*0.04*	*0.04*	*0.07*	*0.06*	*0.01*	*0.07*	*0.00*	*0.00*	*0.00*	*0.04*	*0.04*	*0.00*	*0.00*	*0.08*	*1.08*
38.3 m	Chl[a]	1	repr. anal.	3.30	0.70	1.87	2.06	0.00	1.49	0.00	0.00	0.00	4.71	5.42	0.00	0.00	2.57	41.95
13.0 m	Chl[b]	1	repr. anal.	3.47	0.53	1.87	1.67	0.00	1.70	0.06	0.00	0.05	4.68	5.24	0.11	0.18	2.40	50.49
7.6 m	Chl[b]	1	repr. anal.	3.34	0.66	1.85	1.79	0.00	1.55	0.00	0.00	0.45	4.82	5.18	0.45	0.45	2.51	46.50

n number of the measured grains, *repr. anal.* representative analysis, *SD* standard deviation (with italic), $\sum$ *oct.* sum of octahedral cations, $\sum$ *inter.* sum of the interlayer cations, *t.i.c.* total interlayer charge = 2 × Ca + K + Na, Al^t sum of Al^{IV} and Al^{VI}, *#Mg* Mg/(Mg + Fe^{2+}) × 100

[a] Moderately degraded Chl

[b] Strongly degraded Chl

4.4 EPMA data

Mean compositions and representative structural formulae of white micas and chlorites of the selected four samples determined by EPMA are given in Tables 4 and 5, respectively.

Backscattered electron (BSE) images (Fig. 5a, b) show microstructural relations of the foliated regional metamorphic matrix (indicated by I) and the post-metamorphic coarser-grained layers, lenses without any preferred orientation of grains and flakes. Figure 5c is a part from the foliated matrix with some muscovite/chlorite stacks.

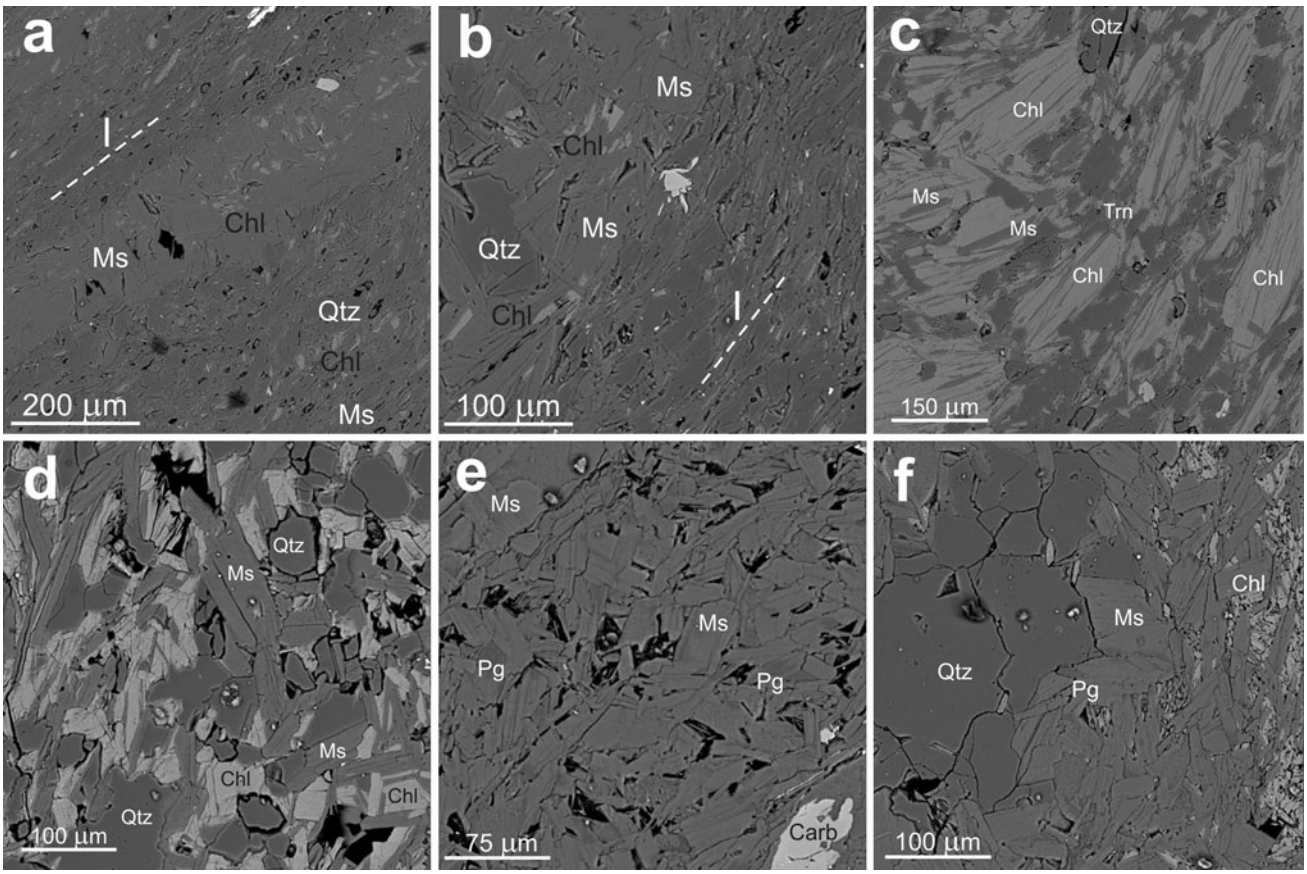

Fig. 5 Microstructural relations (BSE images of sample 75.0 m) (**a**–**d**) and sample 38.3 m (**e**–**f**). For explanation see the text. Abbreviations as in Fig. 4, *Trn* tourmaline

Figure 5d shows a typical part of the randomly arranged post-metamorphic aggregates consisting of muscovite, chlorite, and quartz.

There are no systematic and significant chemical differences between the muscovite grains found in the regional metamorphic foliated matrix (I) and those of the post-metamorphic aggregates in *sample 75.0* m. Paragonite is not found in this sample but muscovite has elevated Na content (often >0.16 atoms per formula unit, a.p.f.u. hereafter, max. 0.22 and min. 0.10). Si content is varying between 3.04 and 3.16 a.p.f.u. while Al is 2.67–2.86 a.p.f.u. Mg is low, rarely exceeds 0.10, Fe is varying between 0.05 and 0.16 a.p.f.u. The $Mg/(Mg + Fe^{2+})$ ratio is between 0.29 and 0.72. Chlorite is Fe-rich with a $Mg/(Mg + Fe^{2+})$ ratio around 0.4 and more homogeneous compositionally than muscovite. Ca, Na, and K are practically lacking in chlorite (Table 5). A complex Fe–Mg–Ca phase, presumably ankerite has been analysed.

In the post-metamorphic aggregates of *sample 38.3* m (Fig. 5e, f), muscovite is Na-rich, similarly to sample 75.0 m. Fe is less than 0.06 and Mg is between 0.03 and 0.06 a.p.f.u. Discrete paragonite grains are present in these parts of the sample. They are Fe- and Mg-free with relatively higher Al content than the muscovite (3.00–3.04 compared to 2.95–3.01). Chlorite is Si-rich and has lower Fe and Mg contents compared to sample 75.0 m. The rare carbonate contains also Mn in addition to Ca, Mg, and Fe in this sample.

In *sample 13.0* m that shows the microstructural features of strongest post-metamorphic alteration, muscovite is strongly degraded having very low K and Na contents. Fe is quite the same as in the other samples while Mg is practically zero. The mixed-layered phase after chlorite is Fe-poor and Si-rich and is characterized by increased amounts of impurities like Ca and Na.

In *sample 7.6* m no paragonite was found with EPMA, but muscovite has high Na content and there is a paragonite-dominant mixed Na–K-white mica as well with 0.54 a.p.f.u. Na and 0.23–0.24 a.p.f.u. K. Fe is higher than 0.05, while Mg is between 0.02 and 0.03 a.p.f.u. in this phase (Table 4). The mixed-layered mineral after chlorite is Si- and Mg-rich and Fe-poor, with considerable amounts of Na impurities.

4.5 TEM observations

The four samples studied by EPMA were also characterized with HRTEM, which allowed a more detailed study of

mineral relations, textures, and phyllosilicate compositions. The mean phyllosilicate compositions and their statistical parameters are given in Table 6 and the compositional relations of dioctahedral white micas analyzed by the AEM with indication of the main compositional vectors are represented in Fig. 6.

Chemical data of *sample 75.0* m confirm the absence of paragonite and the presence of Na-rich K-white micas (Na = 0.11–0.23 a.p.f.u., Fig. 6a) in agreement with the EPMA data. Chlorite analyses from sample 75.0 m are very heterogeneous with a wide range for Fe (1.57–2.43 a.p.f.u.) and a sum of octahedral cations from 5.20 to 5.75 a.p.f.u., however analyses with very low interlayer content give a similar composition to those detected by EPMA (Table 6, analysis 27). Minor amounts of interlayer cations (K, Na and Ca) have been detected suggesting a possible interstratification of smectite layers within the chlorite, which must be responsible of the chemical variation. Smectite interstratification is supported by the *hk*0 selected-area electron diffraction (SAED) pattern of chlorite as well (Fig. 7). The light diffraction ring at ca. 4.5 Å over the chlorite reflections proves turbostratic structure characteristic of smectite. Not in vain, small amounts of Al-smectites have also been analysed with high Si content (>3.84 a.p.f.u.) and low Al content (≤1.50 a.p.f.u.).

The predominant phyllosilicates in the *sample 38.3* m are chlorite and white micas (mainly mixed Na–K mica and paragonite, Fig. 6a). The high resolution images of chlorite (Fig. 8) show defects (layer terminations, fissures, kinks, and wavy layers). There are narrow voids affecting to the continuity of the layers and suggesting the intercalation of one or two layers of other phyllosilicate. In some lattice fringe images periodicities higher than 14 Å can be observed (Fig. 8a). Packet sizes vary from several hundreds to more than a thousand ångstroms. These trioctahedral chlorites have a high Fe content corresponding to a

Table 6 Mean compositions and statistical parameters based on AEM analyses of phyllosilicates

Sample	Mineral	n		Si	Al^{IV}	Al^{VI}	Ti	Fe^{2+}	Mg	Ca	K	Na	∑ oct.	∑ inter.	Al^t	#Mg
75.0 m	Ms	6	Mean	3.15	0.85	1.84	0.01	0.11	0.08	0.00	0.73	0.13	2.03	0.87	2.69	39.32
			SD	*0.07*	*0.07*	*0.08*	*0.01*	*0.02*	*0.03*	*0.01*	*0.20*	*0.05*	*0.08*	*0.22*	*0.13*	*9.70*
38.3 m	Ms	3	Mean	3.03	0.97	1.93	0.01	0.07	0.08	0.02	0.60	0.14	2.09	0.76	2.89	37.88
			SD	*0.04*	*0.04*	*0.06*	*0.00*	*0.00*	*0.10*	*0.00*	*0.16*	*0.06*	*0.05*	*0.11*	*0.08*	*30.71*
	Pg	8	Mean	3.11	0.89	1.93	0.01	0.05	0.04	0.01	0.15	0.67	2.03	0.83	2.82	26.56
			SD	*0.23*	*0.23*	*0.13*	*0.02*	*0.03*	*0.05*	*0.01*	*0.08*	*0.13*	*0.04*	*0.11*	*0.35*	*30.04*
7.6 m	Ms[a]	9	Mean	3.26	0.74	1.91	0.00	0.06	0.09	0.00	0.49	0.16	2.07	0.65	2.66	60.09
			SD	*0.11*	*0.11*	*0.05*	*0.00*	*0.02*	*0.03*	*0.00*	*0.14*	*0.13*	*0.03*	*0.18*	*0.10*	*14.97*
	Pg[a]	4	Mean	3.13	0.87	1.93	0.00	0.05	0.05	0.00	0.22	0.62	2.03	0.84	2.80	50.71
			SD	*0.18*	*0.18*	*0.06*	*0.00*	*0.02*	*0.01*	*0.00*	*0.19*	*0.11*	*0.08*	*0.14*	*0.22*	*7.05*
75.0 m	Chl	4	Mean	3.14	0.86	1.81	0.00	2.03	1.62	0.02	0.03	0.05	5.48	0.10	2.66	44.79
			SD	*0.23*	*0.23*	*0.17*	*0.00*	*0.45*	*0.13*	*0.02*	*0.04*	*0.02*	*0.23*	*0.08*	*0.16*	*6.63*
		Analysis 27		2.83	1.17	1.66	0.00	2.40	1.67	0.00	0.00	0.02	5.75	0.02	2.83	40.94
38.3 m	Chl	3	Mean	3.12	0.88	1.65	0.09	2.37	1.40	0.01	0.04	0.06	5.44	0.10	2.53	37.06
			SD	*0.10*	*0.10*	*0.06*	*0.04*	*0.12*	*0.05*	*0.01*	*0.04*	*0.10*	*0.07*	*0.12*	*0.09*	*2.03*
75.0 m	Sm	2	Mean	3.88	0.12	1.24	0.00	0.35	0.36	0.22	0.19	0.08	1.95	0.50	1.36	51.02
			SD	*0.04*	*0.04*	*0.17*	*0.00*	*0.07*	*0.03*	*0.20*	*0.01*	*0.04*	*0.13*	*0.23*	*0.21*	*6.65*
7.6 m	Sm	7	Mean	3.39	0.61	1.63	0.00	0.32	0.22	0.02	0.20	0.10	2.17	0.33	2.24	44.32
			SD	*0.26*	*0.26*	*0.37*	*0.00*	*0.30*	*0.20*	*0.03*	*0.19*	*0.11*	*0.18*	*0.19*	*0.38*	*22.50*
13.0 m	Hys	13	Mean	3.95	0.00	3.86	–	0.15	0.04	0.01	0.01	0.07	4.05	0.09	3.86	–
			SD	*0.15*	*0.00*	*0.17*	–	*0.14*	*0.03*	*0.02*	*0.01*	*0.06*	*0.19*	*0.06*	*0.17*	–
7.6 m	Kln	2	Mean	3.98	0.00	3.85	–	0.13	0.04	0.00	0.00	0.05	4.02	0.06	3.85	–
			SD	*0.16*	*0.00*	*0.08*	–	*0.12*	*0.03*	*0.00*	*0.00*	*0.08*	*0.17*	*0.08*	*0.08*	–
	Hys	3	Mean	3.91	0.00	3.80	–	0.21	0.12	0.00	0.00	0.04	4.14	0.04	3.80	–
			SD	*0.10*	*0.00*	*0.26*	–	*0.11*	*0.15*	*0.00*	*0.01*	*0.06*	*0.10*	*0.07*	*0.26*	–

White-micas (Ms, Pg) and smectites (Sm) normalized to $O_{10}(OH)_2$; chlorites (Chl) and kaolinite minerals (Hys, Kln) normalized to $O_{10}(OH)_8$

n number of the measured grains, SD standard deviation (with italic), ∑ *oct.* sum of octahedral cations; ∑ *inter.* sum of the interlayer cations, Al^t sum of Al^{IV} and Al^{VI}, *#Mg* Mg/(Mg + Fe^{2+}) × 100

[a] Finely intergrown Ms and Pg phases

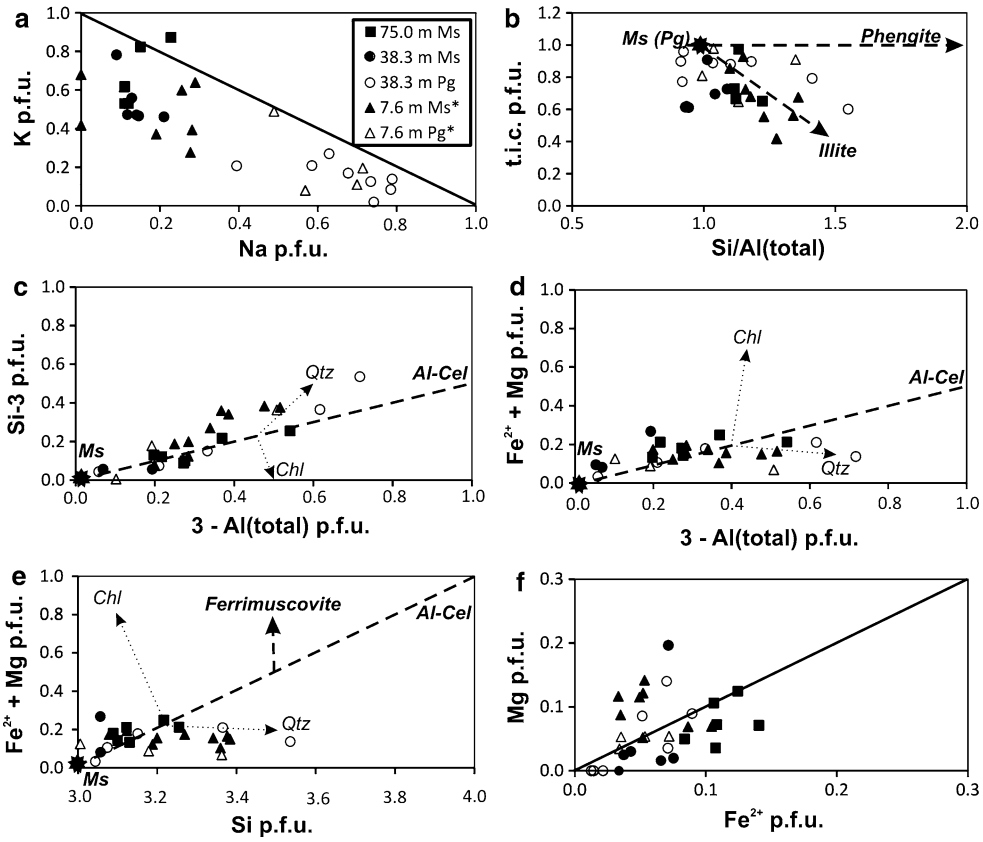

Fig. 6 Compositional relations of dioctahedral white micas. Cation numbers and ratios calculated from AEM analyses. For explanations see the text. In **c–e** compositional parameters suggested by Guidotti and Sassi (1998) are used. t.i.c. = total interlayer charge = K + Na + 2Ca per formula unit. *Small arrows* with fine *dotted lines* indicate the effects of possible contaminations with other minerals, while dashed lines show the isomorphic substitutions within the mica structure. Ms* and Pg* indicate finely intergrown Ms and Pg phases or K–Na mixed white micas (MWM) with K or Na dominancy in the interlayer space

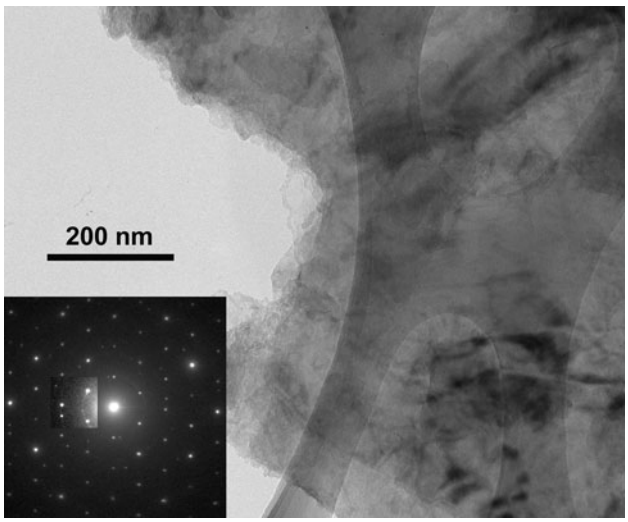

Fig. 7 Bright field (BF) image of chlorite and the corresponding hk0 SAED pattern. The light diffraction ring over the c. 4.5 Å chlorite reflections is heightened in the box (sample 75.0 m)

chamosite variety (Table 6). Most of the analyses show a large range of excess Al^{VI} (up to 0.63 a.p.f.u.) over Al^{IV}. The sum of octahedral cations is around 5.50 a.p.f.u. and a slight contamination by interlayer cations (K, Na, and Ca) has been detected in the chlorite analyses. These data are, at least in part, the result of interstratification of smectite layers within the chlorite, as previously have been shown in lattice fringe images (Fig. 8) and described in the XRPD section.

The lattice fringe images corresponding to paragonites or paragonite-dominant Na–K-white micas are characterized by well-defined and thick packets with few defects. SAED patterns confirm a 2*M* polytype (Fig. 9). AEM analyses are characterized by a K content around 0.20 a.p.f.u. and a Na content of 0.40–0.70 a.p.f.u. The interlayer cation sum is quite variable with a range from 0.60 to 0.90 a.p.f.u. (Fig. 6b). Al content is high whereas Fe + Mg is ≤0.20 a.p.f.u. (Fig. 6c–e). In relation to the muscovite-dominant Na–K micas, the chemical features are very similar with the only obvious difference in the Na and K contents.

Sample 13.0 m, which has been described as the most intense altered sample of the sequence, studied under the TEM shows a mineral composition mainly characterized by the presence of kaolinite group minerals. The predominant mineral in the clay fraction is halloysite, but some large illite and kaolinite platelets can also be seen (Fig. 10). Halloysite exhibits quite particular tubular shape (Fig. 11a, c). It seems to form tubes with only a few number of rolled layers lengthwise straight-cut tubes. The length of these tubes varies within a wide range (≈400–2,800 nm) and the width

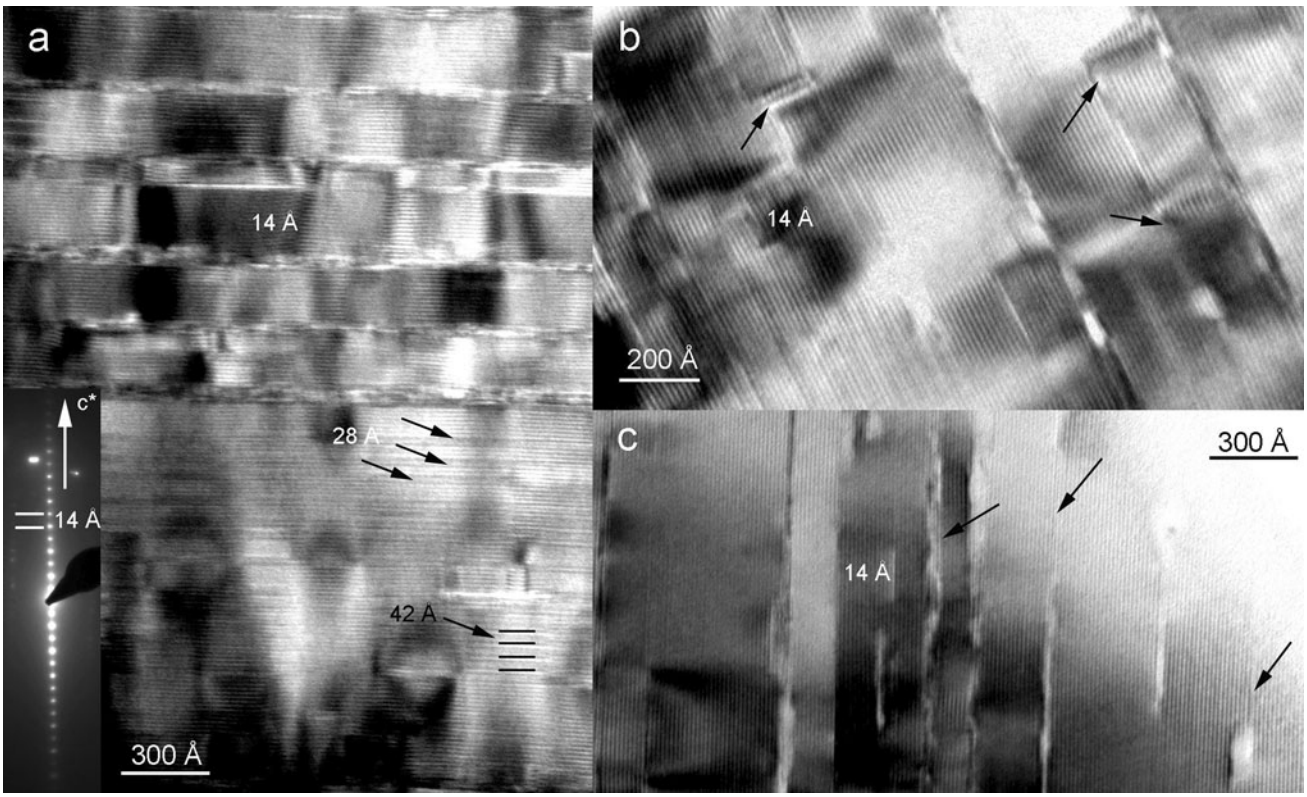

Fig. 8 Lattice-fringe images of chlorite with fissures, contrast changes, wavy layers, and layer periodicities at 28 and 42 Å (**a**); layer terminations and kinks (**b**); intercalation of one or two layers of less thick than 14 Å (*see arrows*) (**c**) (sample 38.3 m)

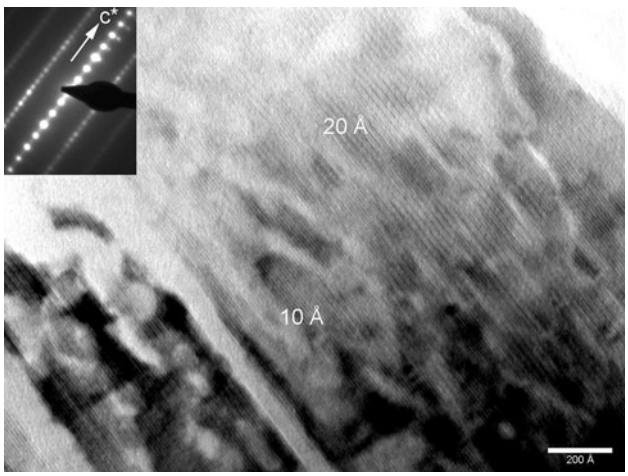

Fig. 9 Lattice-fringe image of part of a 2*M* paragonite crystal (sample 38.3 m)

(diameter) of the tubes varies 40 to 150 nm. The chemical composition of the halloysites is close to 1:1 Si–Al ratio (Table 6). However, all analysed halloysite grains contain some iron. The Fe content varies between 0.05 and 0.57 a.p.f.u., with a mean value of 0.15. Kaolinite, which is distinguished from halloysite by its platy shape also contains 0.10 a.p.f.u. Fe. The amount of kaolinite is far subordinate as compared to halloysite.

Sample 7.6 m produces lattice fringe images of white mica crystals with 10 and 20 Å periodicities; the latter confirms the 2*M* polytype determined by SAED patterns. The mica grains are well-defined several hundred ångstrom thick parallel packets. Chemical data indicate the presence of illites (interlayer-cation-deficient micas, according to Rieder et al. 1998), Na–K micas with Na contents around 0.25 a.p.f.u., and paragonites (Table 6; Fig. 6a, b). The phengitic content is low (<0.20 a.p.f.u.) and disregarding the nature and sum of the interlayer cations, all micas show similar compositional characteristics. Although SAED patterns reveal reflections of a 7.3 Å phase (kaolinite, Fig. 11b), the 7 Å lattice fringes are difficult to observe, due to the quick beam damage. AEM analyses corroborate the presence of these hydrous Al-silicates, primarily halloysite with a constant presence of Fe in the analyses (Table 6).

In addition, 24 Å (10 + 14 Å) periodicities have been detected (Fig. 12). This observation is coherent with the XRPD results in which the 12 and 8 Å peaks were interpreted as the second and third order reflections of a 24 Å superstructure. Chemical analyses for these areas have been normalized to $O_{20}(OH)_{10}$ and correspond to

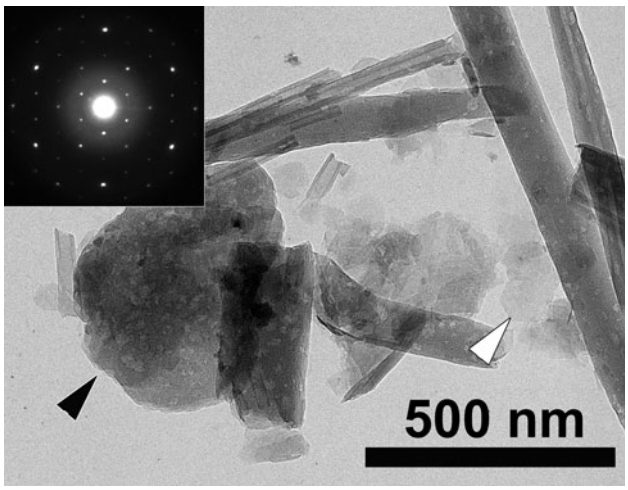

Fig. 10 Aggregate of kaolinite platelets (*black arrowhead*) and an individual kaolinite crystal exhibiting its typical hk0 morphology (*white arrowhead*) among halloysite tubes. The insert shows hk0 SAED pattern of a kaolinite single cystal (sample 13.0 m)

mixed-layers with an intermediate composition between muscovite and chlorite (Table 7), and in some cases, with small amounts of mixed-layered 14 Å (smectitic) component, having Ca, K, and Na (Fig. 13).

AEM analyses of smectites from this sample reveal a wide compositional interval for Al (1.79–2.74 a.p.f.u.), Mg (0.03–0.56 a.p.f.u.), and Fe (0.03–0.79 a.p.f.u.). Some of these analyses can be a mixture of di- and trioctahedral smectite with the predominance of the first one. Traces of calcite, dolomite, rutile grains, quartz, and Fe-oxides have also been detected by TEM in this sample.

5 Discussion

5.1 Regional metamorphic conditions

The KI values (0.22–0.25 $\Delta°2\theta$) and their average from the lower, paragonite-free part of the profile (from 52.0 m downwards) unequivocally indicate epizonal (greenschist facies) regional metamorphic conditions (Table 2). The ChC(001) values of the lower part fall also to the epizone, while ChC(002) values scatter around the boundary between the anchi- and epizone. If the chlorite "crystallinity" indices of sample 52.0 m are excluded because of the partial alteration of chlorite, the ChC(002) values of the lower part indicate also epizonal conditions (mean = 0.230 $\Delta°2\theta$, SD = 0.028 $\Delta°2\theta$, n = 4).

The K-white mica *b* cell dimensions vary between 8.989 and 8.992 Å, indicating low-pressure (high thermal gradient) metamorphic conditions (see Guidotti and Sassi 1976, 1986).

The mineral chemical features of the metamorphic muscovites and chlorites, i.e., the relatively high interlayer charge (occupancy) and low alumino-celadonitic (phengitic) substitution in K-white mica (Fig. 6b–e) and the very low interlayer occupancy (minimal or no swelling mixed-layering) in chlorite as well as the chemical invariability of these minerals are in agreement with the XRPD-based metamorphic zone- and pressure range-indicating parameters. All these unequivocally prove low pressure-type epizonal (greenschist facies chlorite zone, locally, maximum biotite zone) regional metamorphism, confirming the earlier conclusions of Árkai (1977a, b, 1983).

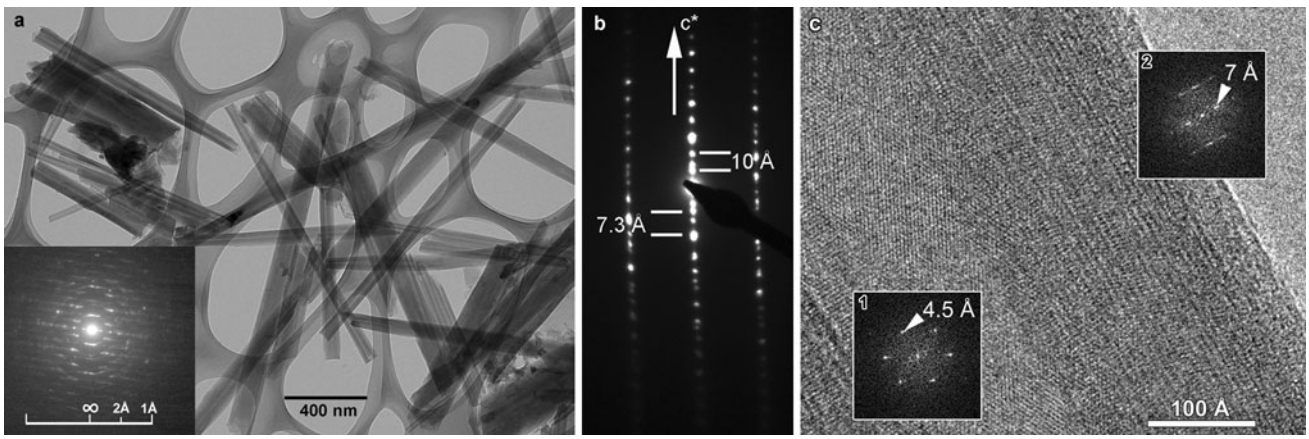

Fig. 11 TEM image and SAED pattern of halloysite (sample 13.0 m) (**a**). SAED pattern with reflections of two phases: mica (10 Å) and kaolinite (7.3 Å) (sample 7.6 m) (**b**) and high resolution image of the rolled 7 Å phase. **c** The Fourier transform of ca. 100 Å × 100 Å area in the middle (*1*) of the tube shows *hk0* projection, while at the border (*2*) proves the 7 Å periodicity along *c** (sample 13.0 m)

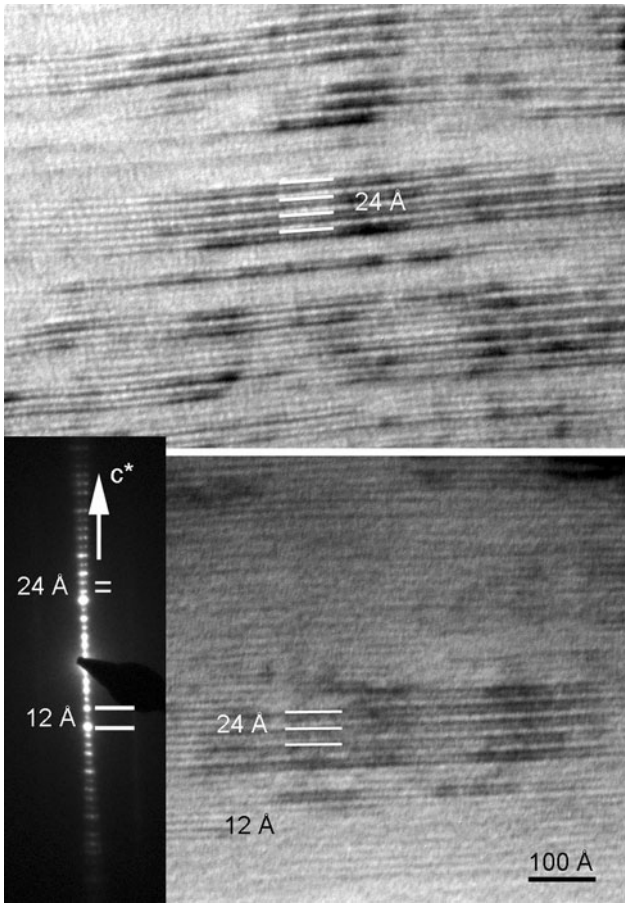

Fig. 12 Lattice-fringe images with layers at 24 Å, confirmed by the SAED pattern. Microanalysis corresponds to muscovite/chlorite mixed-layers (Table 7 analysis r4) (sample 7.6 m)

5.2 Evidence of post-metamorphic alterations

5.2.1 Textural evidence

Petrographic microscopic observations demonstrated that even the freshest parts of the investigated slate sequence show initial forms of post-metamorphic fracturing, "loosening" of the metamorphic microstructure characterized by crenulation cleavage. As the fracturing became more intense, post-metamorphic fluids should have penetrated the slates completely. The rocks that show only embrional forms of post-metamorphic alterations are characterized by metamorphic assemblages that contain quartz + muscovite + chlorite + albite ± calcite, pyrite, and rutile. The formation of paragonite and mixed Na–K-white mica (MWM) were mostly at the expense of albite and the mixed-layered clay mineral (ML) probably formed at the expense of chlorite. ML in traces were found in the lower (relatively fresh) part of the profile, but became significant in the upper part, where chlorite was practically lacking. At lower temperatures discrete swelling phases (predominantly smectite, sporadically vermiculite in sample 13.0 m) also formed.

In the most fractured, loosened zones (channels) of the sequence intense post-metamorphic migration of even low-T fluids caused predominantly halloysite crystallization (with subordinate kaolinite) and most of the already mentioned other post-metamorphic and metamorphic phyllosilicates that could be found in low quantities. Mineral evidence of the post-metamorphic alterations will be discussed in detailed later on this section.

Table 7 Representative chemical compositions for muscovite-chlorite mixed-layers normalized to $O_{20}(OH)_{10}$ (AEM data)

Sample	Point		Si	Al^{IV}	Al^{VI}	Ti	Fe^{2+}	Mn	Mg	Ca	K	Na	∑ oct.	∑ inter.	Al^t	#Mg
7.6 m	r7		6.56	1.44	2.52	0.00	2.63	0.00	2.67	0.08	0.61	0.57	7.83	1.26	3.97	50.39
	r8		6.36	1.64	2.55	0.00	2.60	0.00	2.68	0.08	0.66	0.70	7.82	1.44	4.19	50.79
	r12		6.67	1.33	2.85	0.00	2.86	0.00	2.19	0.17	0.17	0.34	7.90	0.68	4.18	43.44
	g11		6.19	1.81	2.34	0.00	3.98	0.04	2.01	0.00	0.75	0.00	8.36	0.75	4.14	33.57
	g18		6.46	1.54	3.13	0.00	3.56	0.04	1.28	0.12	0.25	0.00	8.02	0.37	4.68	26.50
	g19		6.66	1.34	2.76	0.00	3.06	0.04	2.28	0.04	0.26	0.00	8.14	0.30	4.10	42.64
	r4		6.76	1.24	2.72	0.00	2.79	0.00	2.34	0.00	0.58	0.25	7.85	0.83	3.96	45.53
	r5		6.16	1.84	2.38	0.00	2.87	0.00	2.91	0.00	0.76	0.38	8.16	1.14	4.22	50.36
	r6		6.47	1.53	2.52	0.00	2.80	0.00	2.75	0.08	0.44	0.35	8.07	0.87	4.05	49.62
	r7		6.71	1.29	2.58	0.00	2.83	0.00	2.54	0.04	0.55	0.21	7.96	0.80	3.87	47.29
		Mean	**6.50**	**1.50**	**2.64**	**0.00**	**3.00**	**0.01**	**2.37**	**0.06**	**0.50**	**0.28**	**8.01**	**0.84**	**4.14**	**44.01**
		SD	*0.21*	*0.21*	*0.24*	*0.00*	*0.44*	*0.02*	*0.47*	*0.06*	*0.21*	*0.24*	*0.17*	*0.36*	*0.22*	*8.09*

n number of the measured grains, *SD* standard deviation (with italic), Mean (with bold), ∑ *oct.* sum of octahedral cations; ∑ *inter.* sum of the interlayer cations, Al^t sum of Al^{IV} and Al^{VI}, *#Mg* Mg/(Mg + Fe^{2+}) × 100

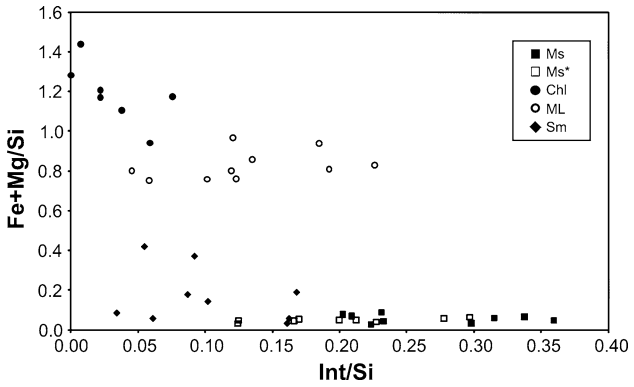

Fig. 13 Chemical variations of muscovite, chlorite, and mixed-layer muscovite-chlorite on the Na + K+Ca/Si versus Fe + Mg/Si diagram. In addition, smectites and Ms* (finely intergrown Ms and Pg phases) were included (all mineral phases analysed by AEM)

5.2.2 *Crystallochemical parameters*

In relation to the metamorphic zone- and pressure-indicating parameters, in the upper, strongly altered part of the profile the KI values and their average are only slightly larger than those of the lower part, indicating somewhat lower apparent metamorphic grade. This means practically that the strong post-metamorphic alteration has caused only weak modifications (loosening or breakup) of the muscovite structure on one hand, and the subordinate amounts of paragonite with overlapping first basal reflection has resulted only in small increase in KI of the 10 Å phase, on the other. The K-white mica *b* cell dimension data of the paragonite-bearing samples from the upper part are only slightly smaller (mean = 8.986 Å, s = 0.003 Å, n = 5), which is in agreement with the theoretical predictions of Guidotti and Sassi (1976, 1986).

5.2.3 *Geochemical variations*

The fluctuations of the major element contents and their relations were attributed partly to the original heterogeneity of the pelitic-silty series in the profile and mostly to the effects of hydrothermal activity that was intense in the upper and moderate to weak in the lower parts of the sequence by Árkai et al. (2008). Opposite changes in SiO_2 and Al_2O_3 contents and relatively high Al_2O_3 content especially in the halloysite- and kaolinite-bearing upper part were observed. The Fe_2O_3 content decreases, the FeO content increases downwards, reflecting oxidation in the late stage of hydrothermal activity and/or influence of near-surface weathering. Neither the Al/(Al + Si) nor the K/(K + Al) and Na/(Na + Al) atomic ratios show systematic differences between the paragonite- (and kaolinite and/or halloysite-) bearing upper and the practically paragonite-free lower parts (see Table 3 of the present paper and Fig. 5 of Árkai et al. 2008).

Summarizing the bulk chemical changes: low-T fluid generally caused decrease in Si, Fe^{2+} and Mg and (relative) increase in Al and Fe^{3+} contents, the final, lowest-T leaching also decreased the amounts of Ca, Na, and K.

5.2.4 *The formation of new mineral phases during retrograde processes*

The main signs of post-metamorphic alterations experienced by this epizonal sequence are the mineral products of which were strongly varying in time and space, also within relatively short distances. Albite and chlorite were almost entirely destroyed and replaced by mainly paragonite, mixed Na–K micas, muscovite-chlorite mixed-layers, halloysite, kaolinite, and smectite.

5.2.4.1 Paragonite and mixed Na–K micas Although the reaction progress of white micas with various interlayer cations in diagenetic and low-T metamorphic regimes characterized by increasing T is fairly well known, the literature contains hardly any data on the behavior, transformations of these minerals in retrograde systems.

As it was documented on a large data set, paragonite and/or mixed Na–K-white mica had not formed during the prograde metamorphism of the Szendrő Paleozoic (Árkai 1983). The paragonite found in the borehole Gn-1 was supposed to be a result of a second metamorphic recrystallization phase by Árkai (1977a). The present—more detailed—study, however arouses serious doubts concerning the regional metamorphic nature of the paragonite in question.

As it is given in Table 1, paragonite is found in subordinate quantities in the upper (intensely retrogressed) part of the profile. In addition, XRPD signals prove the presence of mixed Na–K-white mica in the whole profile, but always in very subordinate (trace) quantities. Figure 14 shows the relative proportions of the three white mica phases (Ms muscovite, Pg paragonite and MWM mixed Na–K-white mica). In the upper part of the profile the relative intensity of the Pg peak reaches c. 10–25 % of that of Ms, while discrete Pg is absent or can be found only as traces in the lower part (Fig. 14a). The proportion of MWM decreases downwards in the profile (Fig. 14b). While Pg dominates over MWM in the upper part, the trace amounts of Na-bearing micas are represented mainly by MWM in the lower part (Fig. 14c).

Neither EPMA nor AEM studies proved Pg in the less altered 75.0 m sample. However, the Ms flakes are rather rich in Na, in average, 0.15 a.p.f.u. on the basis of $O_{10}(OH)_2$ by EPMA and 0.13 a.p.f.u. by AEM (see Tables 4 and 6). The Na/K ratios of the analyzed micas (Fig. 6a) are well

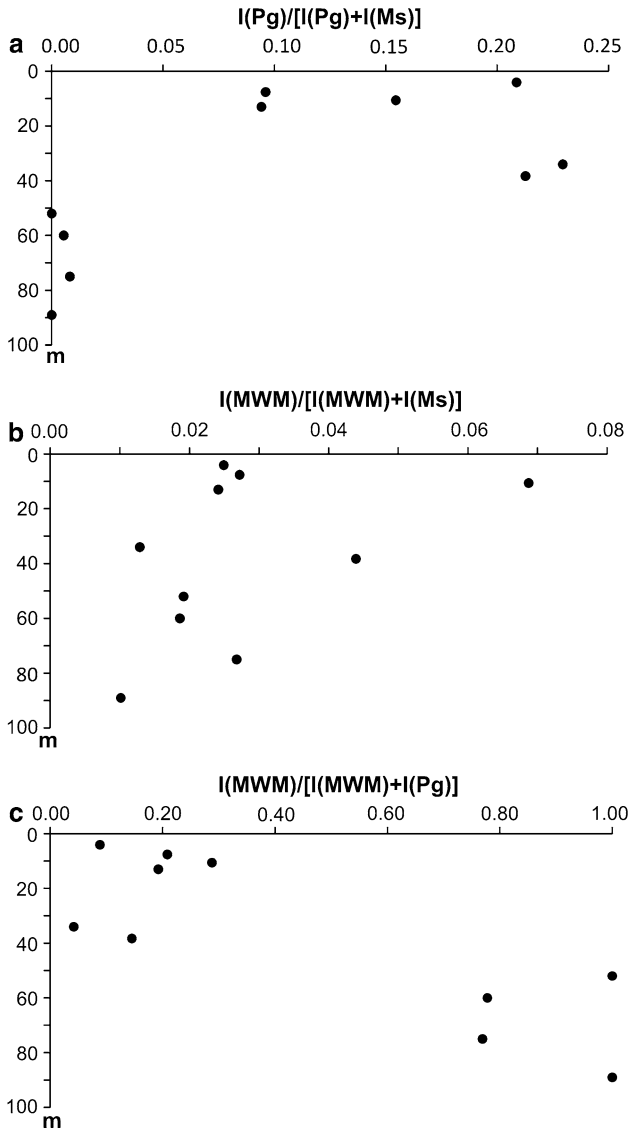

Fig. 14 Comparison between depth and proportions of discrete paragonite (Pg) and mixed Na–K-white mica (MWM) phases related to muscovite (Ms) using the XRPD intensities measured at the near 2-Å part of the <2 μm fraction pattern of each sample. It is supposed that the 10-Å reflection corresponds to Ms, the 9.6-Å reflection to Pg and the 9.8-Å (mostly diffuse) reflection to MWM. For better 2θ resolution the (00,10) reflections were used

within the immiscibility gap determined by Guidotti and Sassi (1998) and cited by Guidotti and Sassi (1976) for the Ms-Pg solvus at epizonal (low-grade) temperature, which in the present case may be around 350 °C. Thus, the mica composition should not be the result of prograde equilibrium crystallization of Ms, but rather a product of post-metamorphic incipient alteration at the expense of albite (see the negative correlation between the appearances and quantities of these minerals given in Table 1). Probably, this retrogression took part at the beginning of the process at relatively high (anchizonal) temperature, and represents an initial, embrional form of incomplete transformation far from the main channels of fluid migration.

As the intensity of post-metamorphic transformation increases (in the series of samples 38.3 → 7.6 → 13.0 m), the total interlayer charge of the Ms decreases and illitic interlayer charges are found. In addition to the Ms, the proportion of MWM and especially, the amounts of Pg increase. In advanced stage of alteration (sample 13.0 m) the Pg content strongly decreases. The K content of Pg is high (is within the immiscibility gap of the Ms–Pg solvus at epizonal conditions), thus implying either non-equilibrium crystallization conditions or intimate parallel intergrowths of Pg and Ms stacks being too thin for correct, separate analyses even for AEM. Interestingly, the Pg has always significantly higher total interlayer charge values than the coexistent Ms (Fig. 6b).

5.2.4.2 Muscovite-chlorite mixed-layers Interstratified phyllosilicates formed by dioctahedral and trioctahedral components are not frequent. In principal, structural reasons related with the different lateral dimensions of both kinds of layers are enough to justify their scarcity in nature, however some cases of illite (muscovite)/chlorite mixed-layers have been described by XRPD, lattice fringe images, and AEM (Lee et al. 1984 and Lee and Peacor 1985, both publications about the same case; Ruiz Cruz 2001; Do Campo and Nieto 2005). The three different cases coincide in terms of: (1) geological context—diagenetic to low-grade metamorphic alteration of pelitic and psammitic materials; (2) XRPD characteristics—rational series of basal reflections corresponding to 24 Å, not affected by conventional clay treatments, i.e. there is no difference between (001), (002) × 2, (003) × 3, etc.; (3) textural characteristics—coexistence of ordered (24 Å) and disordered (random 14 + 10 Å) areas, generally following the foliation direction, and (4) chemical composition—intermediate between those of the chlorites and the micas present in the same sample.

In this research detailed differential diagnosis made by XRPD proved that the muscovite/chlorite mixed-layers (ML) predominantly consists of a mostly regular interstratifications of muscovite and chlorite with usually subordinate amounts of also mixed-layered swelling 14-Å (vermiculitic and/or smectitic) component. The ML phase corresponding to the highest part of the studied profile also presents the same four characteristics described in the previous paragraph (see result description; Figs. 12, 13; Table 7). Hence they can be considered an equivalent case to the three previously described cases.

In spite of the coincidence of characteristics, the genetic interpretation given by the authors differs in detail from the three referred cases, but it is coincident in considering the mixed layers as a metastable product linked to non-equilibrium reactions in the context of very-low grade

retrograde or prograde reactions. The ML in borehole Gn-1 is therefore compatible with the conditions of the post-metamorphic alterations and probably are linked in some way with the chlorite, present in the deeper samples. Chlorite and ML proportions are inversely related along the borehole.

5.2.4.3 Smectite Smectite is present in all the studied samples. It has been detected as a discrete individual component by XRPD (Table 1) and TEM, with a beidellitic composition (Table 6), and as individual layers interleaved in chlorite or in illite-chlorite mixed-layers by TEM/AEM (samples 38.3 m and 7.6 m); such individual layers also affect to the composition of chlorite (Tables 5 and 6) and mixed-layers (Table 7; Fig. 13). The content of smectite does not show any tendency of variation along the sequence, being represented with similar characteristics from the top to the bottom (ca. 90 m). A weathering related origin could be clearly disregarded. But smectite is an incompatible phase with the prograde evolution of the sequence. In addition, the interleaved layers in chlorite and illite-chlorite mixed-layers show textural characteristics at the lattice level indicative of a subsequent alteration process (Fig. 8).

In conclusion, smectite in the present samples shows all the textural and chemical characteristics previously described for other retrograde diagenetic smectites, such as the Malaguide Complex (Nieto et al. 1994) or the South Portuguese Zone (Nieto et al. 2005) and as in those cases its presence is probably related to migration of pervasive fluids at much lower temperatures subsequent to the regional metamorphism far away from the fractures, which justifies its presence in almost all analyzed samples.

5.2.4.4 Halloysite and kaolinite In the upper 40 m of the profile the presence of kaolinite group minerals is constant. This has been corroborated not only by the broad peak at 7.3 Å in the XRPD patterns and the results of the consequent EG and heating treatments of the samples (Fig. 4b, c) but also on the basis of TEM observations (Figs. 10 and 11; Table 6). As in the case of the smectite, previously described, the kaolinite minerals are incompatible with the prograde evolution of the sequence since they are characteristic of diagenetic conditions (Merriman and Peacor 1999).

TEM images have allowed us to distinguish between kaolinite and halloysite particles in function of the shape. According to Hart et al. (2002) the structure and chemical composition of halloysite is similar to that of kaolinite, but both phases are characterised by different morphologies. Kaolinite particles show platy morphologies (Fig. 10) and halloysite particles elongated shapes (Fig. 11a). The tubular halloysite is commonly derived from crystalline minerals, such as feldspars and micas (Singh and Gilkes 1992). The Fe^{3+} content in these mineral phases is very common and according to Brindley et al. (1986), the type of foreign cation present in the kaolinite structure depends mainly on the bulk-rock composition. Table 3 shows the highest Fe_2O_3 contents for the samples with halloysite and kaolinite.

Sample 13.0 m has been described as the strongest post-metamorphic altered sample of the sequence from both, chemical (Table 3) and textural (Fig. 3f) points of view. This sample is characterized by the highest quartz content in the bulk rock fraction and mainly halloysite (with some subordinated kaolinite) in the <2 μm fraction. The main occurrences of halloysite are in weathered or hydrothermally altered rocks, saprolites, and soils. As reviewed by Joussein et al. (2005), halloysite can derive from many rocks, such as granite, gneissic granite, granitic gneiss, gneiss, dolerite, schist, greywacke, green-stone, granodiorite, shale and amphibolite by weathering, pedogenic or hydrothermal processes. The presence of this phase in the upper part of the profile, with the highest amount restricted to the most altered sample (13.0 m) and lower amounts in adjacent samples (from 4.1 to 38.2 m) suggests the circulation of low temperature fluids through fractures in a final stage of the hydrothermal process. The occurrence of subordinate amounts of kaolinite together with halloysite refers to disequilibrium conditions. This affected the sequence producing a gradient from sample 13.0 m (the closest material to the fissures), where the parent minerals had to have a large surface area in contact with the solution and the diffusion to and from the reacting surface had to be fast, downwards. From sample 52.0 m downwards the halloysite is absent and the only low-temperature mineral is smectite.

6 Conclusions

As the crystallochemical parameters (KI, ChC and K-white mica *b* cell dimension) indicate, the Szendrő metapelites were metamorphosed reaching low pressure-type epizonal (greenschist facies) regional metamorphic conditions. But a detailed research of the distribution of mineral assemblages through the vertical section of the borehole as well as the textural disposition of the samples suggest that the formation of paragonite, mixed Na–K micas, chlorite-muscovite ML, smectite and kaolinite-group minerals occurred during a process of retrograde alteration superimposed on the epizonal assemblage.

To account for the distribution of assemblages and textural characteristics we propose that these retrograde minerals had a common origin probably related to the evolution of a hydrothermal alteration process. During an

early stage, the introduction through the fractures and circulation of hydrothermal high-temperature fluids gave rise to the crystallisation of paragonite, mixed Na–K micas and chlorite-muscovite ML under anchizone conditions. The evolution of the hydrothermal fluids towards progressively cooler conditions favoured the formation of smectite, halloysite, kaolinite, and goethite. The major presence of halloysite, subordinate kaolinite, and goethite in the most Si-enriched sample with strong evidence of recrystallization indicates that they were formed in the nearest areas to the circulation conducts of the hydrothermal fluids where an intense leaching of the parent materials was produced. Smectite is not only present in the halloysite and kaolinite samples but also in farther areas, where the influence of the parent rocks had a higher control on the reaction products and the fluid had diminished its reactivity. The Al content required for the formation of beidellitic smectite and halloysite was provided by albite and muscovite dissolution from nearby sites. In addition, as the Fe_2O_3 content increases upwards, this reflects oxidating conditions in the late stage of hydrothermal activity and/or influence of near-surface chemical weathering.

Acknowledgments Financial support has been supplied by the Hungarian National Research Fund (OTKA, Budapest) to P.Á. (Grant No. T-049454, Budapest), the Spanish Ministry of Science (Research Project CGL2011-30153-C02-01) and the Acción Integrada Hispano-Húngara HH2006-0030) and Research Groups RNM 325 and RNM 179 of the Junta de Andalucía. T.N. also acknowledges funding from the Spanish Ministry of Science and Education Mobility Program No. SB2005-0111 and hospitality at University of Jaén (Spain). The authors are indebted to Dr. Susanne Th. Schmidt (Geneva) and an anonymous reviewer as well as to Dr. Sébastien Potel (Lasalle-Beauvais) for their corrections and advices.

References

Abad, I., Jiménez-Millán, J., Molina, J. M., Nieto, F., & Vera, J. A. (2003). Anomalous reverse zoning of saponite and corrensite caused by contact metamorphism and hydrothermal alteration of marly rocks associated with subvolcanic bodies. *Clays and Clay Minerals, 51*, 543–554.

Árkai, P. (1977a). *Comparative mineralogical and petrographical characteristics of the geological key-profiles from the Bükk, Uppony and Szendrő Mountains*. Budapest: Laboratory for Geochemical Research, Hungarian Academy of Sciences (in Hungarian).

Árkai, P. (1977b). Low-grade metamorphism of Paleozoic formations of the Szendrő Mountains (NE Hungary). *Acta Geologica Academiae Scientarium Hungaricae, 21*, 53–80.

Árkai, P. (1982). Incipient regional metamorphism (on the examples of the Bükk, Uppony and Szendrő Mountains, NE-Hungary. Candidate of Science (PhD) Thesis, Budapest (in Hungarian).

Árkai, P. (1983). Very low- and low-grade Alpine regional metamorphism of the paleozoic and mesozoic formations of the Bükkium, NE-Hungary. *Acta Geologica Hungarica, 26*, 83–101.

Árkai, P. (2002). Phyllosilicates in very low-grade metamorphism: Transformation to micas. In A. Mottana, F.P. Sassi, J.B.Jr. Thompson & S. Guggenheim (Eds.), *Micas: crystal chemistry and metamorphic petrology, reviews in mineralogy and geochemistry* (pp. 463–478). Washington: Mineralogical Society of America.

Árkai, P., Balogh, K., & Dunkl, I. (1995a). Timing of low-temperature metamorphism and cooling of the paleozoic and mesozoic formations of the Bükkium, innermost western Carpathians, Hungary. *Geologische Rundschau, 84*, 334–344.

Árkai, P., Ferreiro Mählmann, R., Suchy, V., Balogh, K., Sýkorová, I., & Frey, M. (2002). Possible effects of tectonic shear strain on phyllosilicates: a case study from the Kandersteg area, Helvetic domain, Central Alps, Switzerland. *Schweizerische Mineralogische und Petrographische Mitteilungen, 82,* 273–290.

Árkai, P., Livi, K. J. T., & Horváth, P. (2008). Dioctahedral mixed K-Na-micas and paragonite in diagenetic to low-temperature metamorphic terrains: bulk rock chemical, thermodynamic and textural constraints. *Central European Geology, 51*, 283–314.

Árkai, P., Sassi, F. P., & Sassi, R. (1995b). Simultaneous measurements of chlorite and illite crystallinity: a more reliable tool for monitoring low- to very low-grade metamorphisms in metapelites. A case study from the Southern Alps (NE Italy). *European Journal of Mineralogy, 7*, 1115–1128.

Brindley, G. W., Chih-Chun, K., Harrison, J. L., Lipsicas, M., & Raythatha, R. (1986). Relation between structural disorder and other characteristics of kaolinites and dickites. *Clays and Clay Minerals, 34*, 239–249.

Cliff, G., & Lorimer, G. W. (1975). The quantitative analysis of thin specimens. *Journal of Microscopy, 103*, 203–207.

Do Campo, M., & Nieto, F. (2005). Origin of mixed-layered (R1) muscovite-chlorite in an anchizonal slate from Puncoviscana Formation (Salta Province, Argentina). *Clay Minerals, 40*, 317–332.

Fülöp, J. (1994). *Magyarország geológiája. Paleozoikum II*. Akadémiai Kiadó, Budapest, p. 445 (in Hungarian).

Green-Kelly, R. (1953). The identification of montmorillonoids in clays. *Journal of Soil Science, 4*, 232–237.

Guidotti, C. V., & Sassi, F. P. (1976). Muscovite as a petrogenetic indicator mineral in pelitic schists. *Neues Jahrbuch für Mineralogie Abhandlungen, 127*, 97–142.

Guidotti, C. V., & Sassi, F. P. (1986). Classification and correlation of metamorphic facies series by means of muscovite b data from low-grade metapelites. *Neues Jahrbuch für Mineralogie Abhandlungen, 153*, 363–380.

Guidotti, C. V., & Sassi, F. P. (1998). Petrogenetic significance of Na-K white mica mineralogy: recent advances for metamorphic rocks. *European Journal of Mineralogy, 10*, 815–854.

Hart, R. D., Gilkes, R. J., Siradz, S., & Singh, B. (2002). The nature of soil kaolins from Indonesia and Western Australia. *Clays and Clay Minerals, 50*, 198–207.

Jiménez-Millán, J., Velilla, N., & Vázquez, M. (2007). Deformation promoted defects and retrograde chloritization of biotite in slates from a shear zone, Southern Iberian Massif, SE Spain. *Clays and Clay Minerals, 55*, 284–294.

Joussein, E., Petit, S., Churchman, J., Theng, B., Righi, D., & Delvaux, B. (2005). Halloysite clay minerals—a review. *Clay Minerals, 40*, 383–426.

Kisch, H. J., Árkai, P., & Brime, C. (2004). On the calibration of the illite Kübler index (illite ″crystallinity″). *Schweizerische Mineralogische und Petrographische Mitteilungen, 84*, 323–331.

Kovács, S., Szederkényi, T., Buda, Gy., Császár, G., & Nagymarosi, A. (2000). Tectonostratigraphic terranes in the pre-Neogene basement of the Hungarian part of the Pannonian area. *Acta Geologica Hungarica, 43,* 225–328.

Lee, J. H., & Peacor, D. R. (1985). Ordered 1:1 interstratifications of illite and chlorite. A transmission and analytical electron microscopy study. *Clays and Clay Minerals, 33*, 463–467.

Lee, J. H., Peacor, D. R., Lewis, D. D., & Wintsch, R. P. (1984). Chlorite-illite/muscovite interlayered and interstratified crystals: a TEM/STEM study. *Contributions to Mineralogy and Petrology, 88*, 372–385.

Menuier, A., & Velde, B. (Eds.), (2004). *Illite. Origins, evolution and metamorphism.* Berlin: Springer.

Merriman, R. J. (2005). Clay minerals and sedimentary basin history. *European Journal of Mineralogy, 17*, 7–20.

Merriman, R. J., & Frey, M. (1999). Patterns of very low-grade metamorphism in metapelitic rocks. In M. Frey & D. Robinson (Eds.), *Low grade-metamorphism* (pp. 61–107). Oxford: Blackwell Science.

Merriman, R. J., & Peacor, D. R. (1999). Very low-grade metapelites: mineralogy, microfabrics and measuring reaction progress. In M. Frey & D. Robinson (Eds.), *Low grade-metamorphism* (pp. 10–60). Oxford: Blackwell Science.

Németh, T., Berényi Üveges, J., Michéli, E. & Tóth, M. (1999). Clay minerals in paleosols at Visonta. *Acta Mineralogica-Petrographica, 40,* 11–19.

Nieto, F., Mata, P., Bauluz, B., Giorgetti, G., Árkai, P., & Peacor, D. R. (2005). Retrograde diagenesis, a widespread process on a regional scale. *Clay Minerals, 40*, 93–104.

Nieto, F., & Peacor, D.R. (1993). Regional retrograde alteration of prograde lower grade hydrated assemblages. *Terra Abstracts,* 419, Suppl 1, Terra Nova Vol. 15.

Nieto, F., Velilla, N., Peacor, D. R., & Ortega-Huertas, M. (1994). Regional retrograde alteration of sub-greenschist facies chlorite to smectite. *Contributions to Mineralogy and Petrology, 115*, 243–252.

Rieder, M., Cavazzini, G., D' Yakonov, Y.S., Kamanetskii, V.A.F., Gottardi, G., Guggenheim, S., Koval, P.K., Müller, G., Neiva, A.M.R., Radoslovich, E.W., Robert, J.L., Sassi, F.P., Takeda, H., Weiss, Z., & Wones, D.R. (1998). Nomenclature of the micas. *Canadian Mineralogist, 36,* 1–8.

Ruiz Cruz, M. D. (2001). Mixed-layer mica-chlorite in very low-grade metaclastites from the Malaguide Complex (Betic Cordilleras, Spain). *Clay Minerals, 36*, 307–324.

Siivola, J., & Schmid, R. (2007) List of mineral abbreviations. In D. Fettes & J. Desmons, (Eds.), *Metamorphic rocks: a classification and glossary of terms* (pp. 93–110). Cambridge: Cambridge University Press.

Singh, B., & Gilkes, R. J. (1992). An electron optical investigation of the alteration of kaolinite to halloysite. *Clays and Clay Minerals, 40*, 212–229.

Taylor, S.R., & McLennan, S.M. (1985). *The continental crust: its composition and evolution*. Oxford: Blackwell Science.